International Journal of Nanomedicine

Dovepress
open access to scientific and medical research

Open Access Full Text Article

REVIEW

Magnetic polymeric nanoassemblies for magnetic resonance imaging-combined cancer theranostics

This article was published in the following Dove Press journal:
International Journal of Nanomedicine

Shenglong Gan[1,2,*]
Yisheng Lin[3,*]
Yancong Feng[1,2]
Lingling Shui[1,2]
Hao Li[1,2]
Guofu Zhou[1,2]

[1]Guangdong Provincial Key Laboratory of Optical Information Materials and Technology and Institute of Electronic Paper Displays, South China Academy of Advanced Optoelectronics, South China Normal University, Guangzhou, Guangdong 510006, [2]National Center for International Research on Green Optoelectronics, South China Normal University, Guangzhou, Guangdong 510006, [3]Department of Radiology, The First Affiliated Hospital, Guangzhou University of Traditional Chinese Medicine, Guangzhou, Guangdong 510405, China

*These authors contributed equally to this work

Correspondence: Hao Li; Lingling Shui
No. 378, West Waihuan Road, Bld. 5, SCNU, Guangzhou Higher Education Mega Center, Guangzhou, Guangdong 510006, China
Tel/fax +86 20 3931 4813
Email haoli@scnu.edu.cn; shuill@m.scnu.edu.cn

Abstract: Cancer has become one of the primary causes of death worldwide. Current cancer-therapy schemes are progressing relatively slowly in terms of reducing mortality, prolonging survival, time and enhancing cure rate, owing to the enormous obstacles of cancer pathophysiology. Therefore, specific diagnosis and therapy for malignant tumors are becoming more and more crucial and urgent, especially for early cancer diagnosis and cancer-targeted therapy. Derived theranostics that combine several functions into one "package" could further overcome undesirable differences in biodistribution and selectivity between distinct imaging and therapeutic agents. In this article, we discuss a chief clinical diagnosis tool – MRI – focusing on recent progress in magnetic agents or systems in multifunctional polymer nanoassemblies for combing cancer theranostics. We describe abundant polymeric MRI-contrast agents integrated with chemotherapy, gene therapy, thermotherapy, and radiotherapy, as well as other developing directions.

Keywords: polymer, nanoassembly, magnetic resonance imaging, cancer theranostics

Introduction

Along with the aging and growth of the world population, cancer is the primary cause of death in economically developed countries and the secondary one in developing countries.[1] In 2017, 1,688,780 new cancer cases and 600,920 cancer deaths were estimated in the USA.[1] A significant proportion of the worldwide cancer issues could be prevented by popularizing cancer knowledge and implementing programs for tobacco and alcohol control, vaccination (for liver and cervical cancers), routine detection and treatment, and promoting physical activity and healthier dietary patterns by public health campaigns.[2] As a key link, the early diagnosis and radical therapy of malignant tumors can obviously improve the survival and even healing probability of cancer patients. Particularly, many novel materials and technologies have been applied to greatly promote therapeutic efficacy for cancer in recent years.

In 2002, the term "theranostic" first appeared, being defined as the multimodal combination of therapy and diagnostic imaging by Funkhouser.[3] It means that therapeutic drugs and imaging agents are packaged at the same dose and transported at the same time. Such a combination of several features into one package may overcome undesirable differences in biodistribution and selectivity existing between distinct imaging and therapeutic agents.[4] For example, chemotherapeutic drugs are considered for cancer treatment. Most of these routine anticancer drugs suffer from poor pharmacokinetics, inappropriate biodistribution, growing multidrug resistance, and widespread toxicity in vivo to a variety of healthy tissue. They are generally unable to accumulate well at the pathological site or cleared out from the circulation easily and rapidly. Consequently,

submit your manuscript | www.dovepress.com
Dovepress
http://dx.doi.org/10.2147/IJN.S164817

many agents that are highly effective in vitro often appear not only relatively ineffective but also toxic when administered in vivo.[5,6] However, after these drugs are integrated into one theranostic system, clearly their visualization by diagnostic imaging is very helpful in real-time gains in important information on diseased tissue, delivery kinetics, and drug efficacy to tune the drug-dosage and treatment protocols. In contrast to adopting a traditional "One size fits all" approach, a "Two or more is better than one" philosophy integrated with multifunctional theranostic systems can work out more individualized solutions to improve curative effect significantly according to patients' real-time condition.[4,5,7] Characteristic features are detailed in Figure 1. These incorporations of contrast agents and pharmacologically active agents into one nanomedicine may allow biodistribution and accumulation to be visualized noninvasively to monitor drug release and response in real time for combined theranostics.

As such, in cancer treatment, therapy and diagnosis are usually integrated into one term: "cancer theranostics". After significant advances over the past several decades, current diagnostic and therapeutic approaches still rely predominantly on invasive (ie, random biopsies and surgery) and crude, aspecific techniques, such as irradiation and chemotherapeutic agents. From a clinical perspective, cancer is almost uniformly fatal.[8] Therefore, there is still an urgent need to improve the susceptibility, accuracy, and specificity of cancer theranostics.

In this review, we focus on various magnetic polymeric nanoassemblies to display the nature of bifunctional or multifunctional MRI-contrast agents from the perspective of their theranostic types, including classification, imaging principles, and specific strategies for high signal sensitivity. Particularly, we introduce magnetic polymeric nanoassemblies into MRI-integrated cancer theranostics combined with chemotherapy, gene therapy, thermotherapy, and radiotherapy, and systematically display their recent development, as shown in Figure 2.

Polymeric nanoassemblies in cancer theranostics

In 1975, a rational model for pharmacologically active polymers was proposed by Ringsdorf.[9] The Ringsdorf model is primarily aimed at covalently bound polymer–drug conjugates, and consists of three components: a polymeric solubilizer, a drug usually bound to a polymer backbone via a linker, and a targeting moiety to guide a drug-delivery system to a determined target. The enhanced permeability and retention effect, defined as the greater permeability of tumor vessels for macromolecules than normal vessels and the impaired clearance of these macromolecules from the interstitial space of the tumor (contributing to longer retention of these molecules), will greatly facilitate polymer–drug conjugates accumulated within desired physiological regions.[10]

The drugs mentioned are not limited to just chemical drug molecules, and the composites of polymer–drug conjugates from interactions among drugs and polymer chains can also be regarded as "drugs". Various drug–polymer hybrids, including polymeric conjugates, composites, dendrimers,

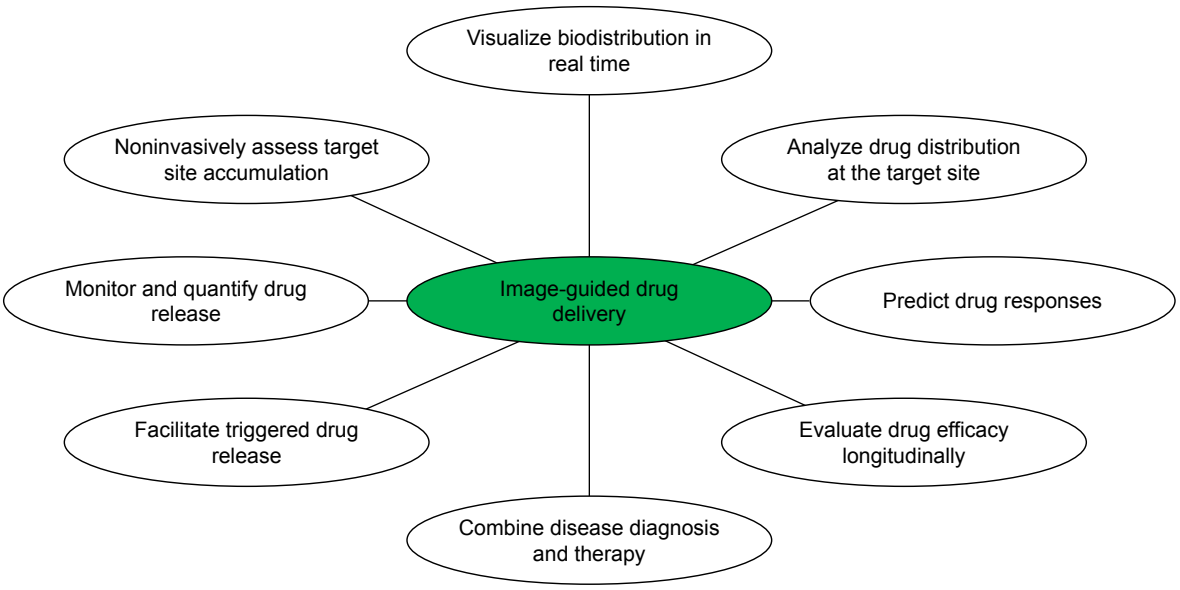

Figure 1 Schematic representation of applications of nanotheranostics and image-guided drug delivery to improve curative effect.
Notes: Reprinted with permission from Lammers T, Kiessling F, Hennink WE, Storm G. Nanotheranostics and image-guided drug delivery current concepts and future direction. *Mol Pharm.* 2010;7:1899–1912.[5] Copyright 2010, American Chemical Society.

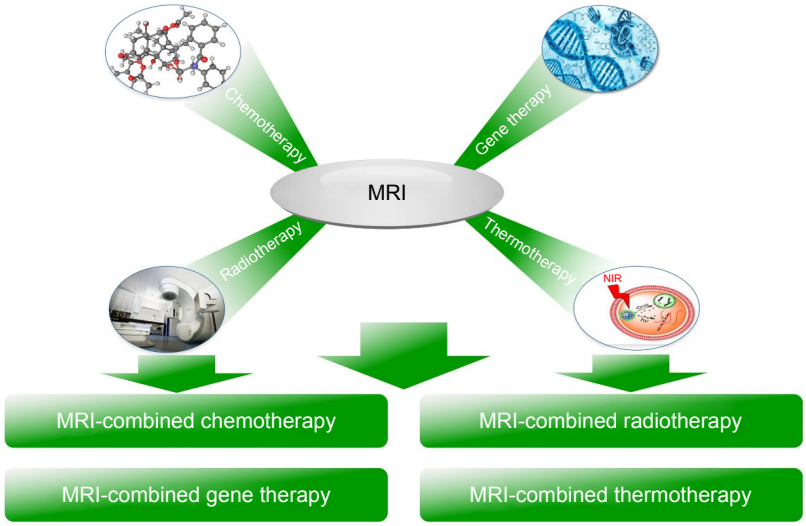

Figure 2 The scheme of bifunctional or multifunctional MRI-contrast agents and their applications.
Abbreviation: NIR, near-infrared.

hydrogel, microspheres, microcapsules, microbubbles, nanospheres, micelles, vesicles, nanorods, and nanowafers, have been used as theranostic polymer agents for cancer management,[10–14] as summarized in Figure 3.

MRI-contrast agents

From a clinical point of view, MRI is one of the most powerful and noninvasive imaging tools for disease diagnosis, widely used in neurological, musculoskeletal, cardiovascular, and oncological imaging. MRI has the advantages of no radiation harm, high sensitivity to blood flow, and yielding great contrast between different soft tissues. Magnetic nanoparticles (MNPs) represent a promising nanomaterial for targeted therapy and imaging.[15] MRI is an effective clinical imaging tool for the theranostics of cancer.

Based on the principle of nuclear MR spectroscopy, MRI images are generated by spatially encoding the nuclear MR signal coming from nuclei (eg, protons) presented in the

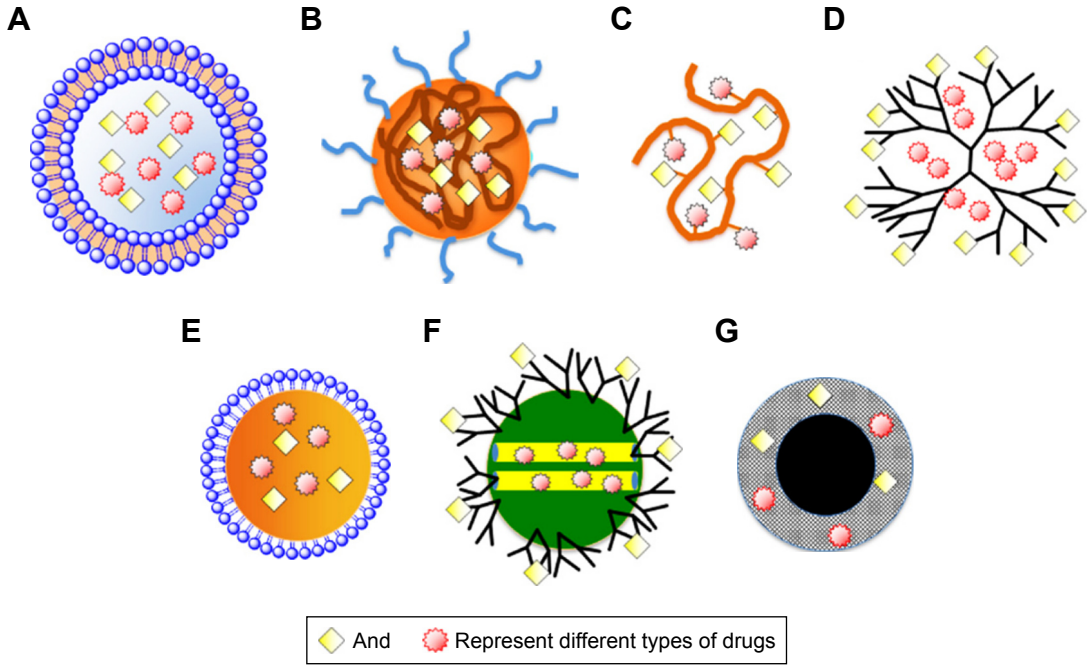

Figure 3 Nanoscale drug carriers used as theranostic polymer agents for cancer management.
Notes: (**A**) Liposomes, (**B**) polymeric micelles, (**C**) polymer–drug conjugate, (**D**) dendrimer, (**E**) nanoemulsion, (**F**) mesoporous silica nanoparticles, and (**G**) iron oxide nanoparticles. Reprinted from *Biochem Pharmacol*, 83, Hu CM, Zhang L, Nanoparticle-based combination therapy toward overcoming drug resistance in cancer, 1104–1111.[11] Copyright 2012, with permission from Elsevier.

object and through the application of time-varying, linear magnetic field gradients.[16] However, MRI contrast is often insufficient in clinical practice. A number of contrast agents have been introduced to enhance image contrast between normal and diseased tissue by increasing the relaxation rates of water protons in tissue in which the agent accumulates, thus being helpful for radiologists to make a more precise diagnosis on the status of organ function or blood flow.[17]

Classification of MRI-contrast agents

The image contrast in MRI is typically classified by its sensitivity to three tissue parameters: proton density, longitudinal (or spin–lattice) relaxation time (T_1), and transverse (or spin–spin) relaxation time (T_2). Currently available MRI-contrast agents can be divided into two classes: T_1 agents and T_2 agents. T_1 agents generally generate positive image contrast by increasing longitudinal relaxation rates ($1/T_1$) of surrounding water protons in tissue more than transverse relaxation rates ($1/T_2$). With conventional pulse sequences, this dominant T_1-lowering effect gives rise to increased signal intensity and predominance on T_1-weighted images. Commonly, Mn^{2+} (LumenHance) and Gd^{3+} (Magnevist enteral and Gadolite) are used as metal centers of the most common T_1 agents. Recently, however, Wei et al[18] designed and developed a gadolinium (Gd)-free T_1-contrast agent with exceedingly small zwitterion-coated superparamagnetic iron oxide NPs (IONPs). Similarly, T_2 agents generally generate negative image contrast by selectively increasing the $1/T_2$ of tissue to decrease in signal intensity and be predominant on T_2-weighted images. Some common T_1/T_2 agents are summarized in Figure 4A, including Gd-DTPA-BMA (OmniScan), Gd-DTPA (Magnevist), Gd-HPDO3A (ProHance), Gd-DO3A–butrol (Gadovist), Mn-DPDP (Teslascan), and Gd-DOTA (Dotarem), Fe_3O_4 NPs, $MnFe_2O_4$ NPs, FeCo NPs, and FePt NPs.

Furthermore, the mechanisms of T_1-weighted imaging and T_2-weighted imaging (γ-Fe_2O_3 and Fe_3O_4 [Lumirem, GastroMark, and Abdoscan] as central moiety of the most common T_2 agents) are shown in Figure 4B.[19–22] Briefly, MRI is the reflection of an atomic magnetic moment after introducing a magnetic pulse. In the absence of an external magnetic field, the proton has a magnetic momentum (ω_0) that deflects from the central axis, as Figure 4B shows. With application of an external magnetic field to the proton, the direction of magnetization will align to the field direction and revert to its original state when the magnetic field disappears, and signals from this process will be collected and changed into MRI images. The process of the system recovered from the excitation state to original state is defined as the relaxation state. In general, the magnetization (M_z) of z-axis (Figure 4B) is called longitudinal relaxation or T_1 relaxation, and the magnetization (M_{xy}) of the xy-plane (Figure 4B) is called transverse relaxation or T_2 relaxation, with reciprocals of T_1/T_2 relaxation defined as r_1/r_2 relaxivity. In biomedicine diagnosis, results are visual output as weighted images, such as T_1- and T_2-weighted images. Signal-intensity formulae of T_1- and T_2-weighted images are shown in Figure 4B. According to the formulae and the curves between magnetization and relaxation time, we can know that the T_1-weighted image will be brighter if T_1 relaxation is short enough, and the T_2-weighted image will be darker if T_2 relaxation is short enough.

Recently, significant progress has been achieved in the development of MRI-contrast systems. This greatly facilitates differentiation of cancerous tissue from surrounding normal tissue by using magnetic fields and radio waves, which might make the early diagnosis of cancer with high accuracy possible.[8,17,18,23] The introduction of various polymer carriers has been carried out to develop crude MRI-contrast agents into multifunctional vector integrated with therapeutic (even diagnostic) approaches for advanced cancer theranostics.

How to increase signal sensitivity

In terms of Solomon–Bloembergen–Morgan theory, T_1-relaxation enhancement depends on four key parameters: hydration number (q; number of labile water molecules coordinated with the metal), residence time (τ_M; lifetime of coordinated water molecules at the metal site), rotational correlation time (τ_R; tumbling motion of the complex), and relaxation characteristics of the unpaired electrons of the metal ion (T_{1E}).[24] The relationship between T_1 relaxivity (r_1^{IS}) and inner-sphere water is described by Equation 1:[25]

$$r_1^{Is} = \frac{q/[H_2O]}{(T_{1m} + \tau_M)} \quad (1)$$

where T_{1m} is the T_1 of the water proton, q hydration number, τ_M residence time, and $[H_2O]$ water concentration (mM). Apparently, both increasing q and decreasing T_{1m} or τ_M would enhance T_1 relaxivity, but the q-value of clinically approved contrast agents is 1 (q=1) for safety. Therefore, the key to designing advanced T_1 agents is to optimize the molecular structure. For example, Gd(III) molecular complexes usually become more labile and behave with decreasing thermodynamic stability and kinetic inertness of Gd ligands and raise toxicity issues, typically once more coordination sites are

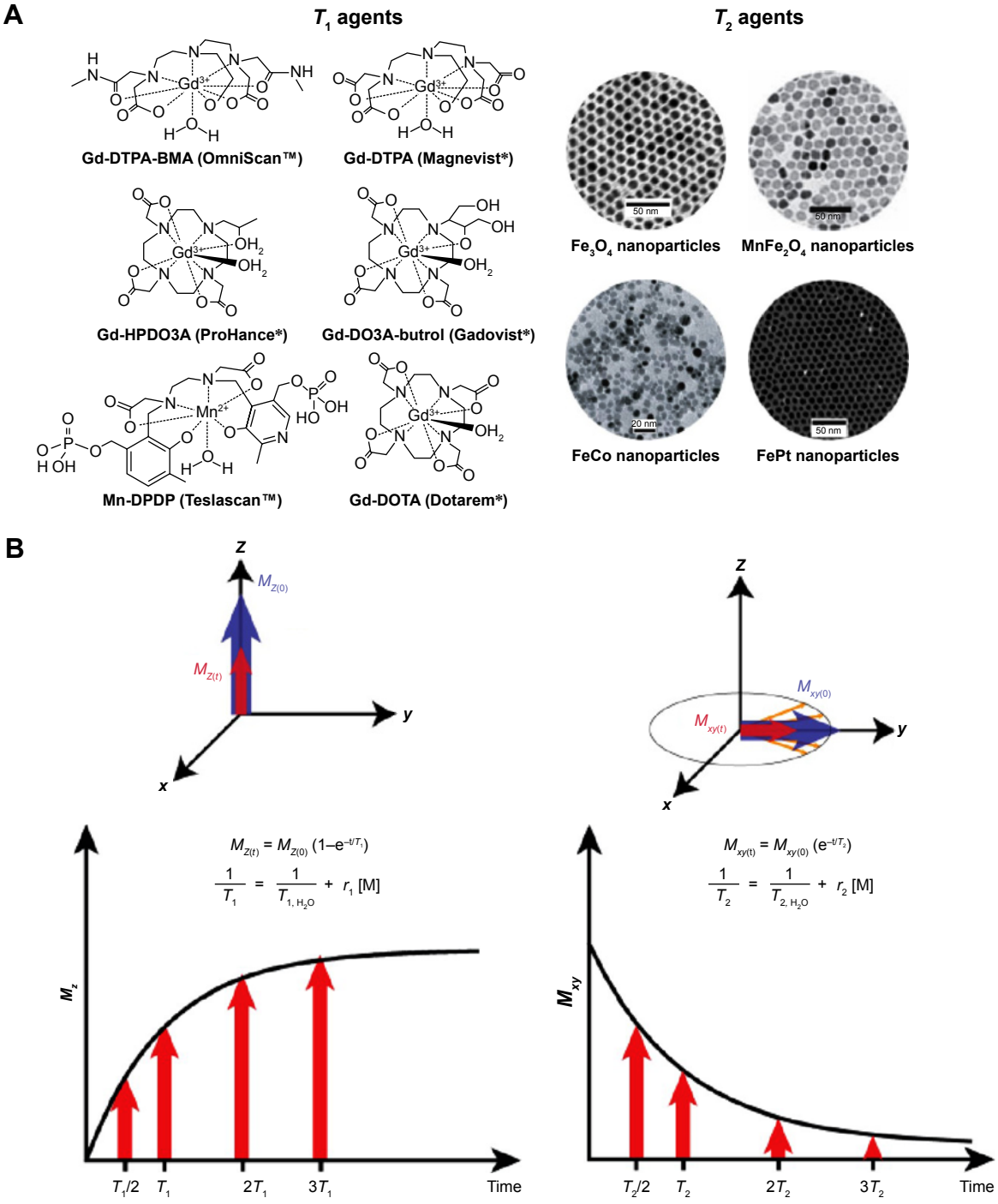

Figure 4 (**A**) Chemical structure of representative T_1 agents (left) and transmission electron microscopy images of exemplary T_2 agents (right). (**B**) T_1 relaxation (left) and T_2 relaxation (right). $M_{z(t)}$, longitudinal magnetization; $M_{z(0)}$, longitudinal magnetization of original equilibrium state; $M_{xy(t)}$, magnetization in the *xy*-plane; $M_{xy(0)}$, magnetization in *xy*-plane of original equilibrium state; $T_{1,H_2O}/T_{2,H_2O}$, relaxation time of pure water; [M], concentration of contrast agent; r_1/r_2, relaxivity. *Gd-DTPA (Magnevist) is a commercial MRI contrast agent like OmniScan™.

Note: Reproduced from Khemtong C, Kessinger CW, Gao J. Polymeric nanomedicine for cancer MR imaging and drug delivery. *Chem Commun (Camb).* 2009:3497–3510.[19] Copyright 2009, with permission of The Royal Society of Chemistry.

Abbreviation: Gd, gadolinium.

opened up for water ligation.[26] Plenty of research has been done focusing on prolonging the rotational correlation time (τ_R) through retarding the tumbling motion of the metal–water proton vector of the system.[27]

For T_2 agents (eg, superparamagnetic Fe_3O_4 NPs), the spin–spin relaxivity (R_2; $1/T_2$) represents the degree of T_2-contrast effect, namely that higher R_2 corresponds with greater contrast effect. At present, the relationship between

NP characteristics and R_2 of the proton could be described by:[28–31]

$$R_2 = \frac{1}{T_2} = \left(\frac{32\pi}{405}\right)\gamma_1^2\mu^2\frac{N_A}{100^o}\left(\frac{M}{rD}\right)\left\{6.5j_2(\omega_s) + 1.5j_1(\omega_s) + 2j_1(0)\right\} \quad (2)$$

and

$$\text{“j”}\downarrow\text{“n”}(\text{“}\omega,T,\text{”“}T\text{”}\downarrow\text{“Sn”})\text{”}=\text{““R”}\downarrow\text{“e”}\ \text{“(“(“1+”“l”/“4”[(“(i}\omega\tau\text{+”“}T\text{”/“}T\text{”}\downarrow\text{“Sn”)”)]}\ \uparrow\text{(“l”/“2”))/(“l+”[(“(i}\omega\text{T+”“}T\text{”/“}T\text{”}\downarrow\text{“Sn””)]}\ \uparrow\text{(“l”/“2”)“+”“4”/(“9”(i}\omega T\text{+”“}T\text{”/“}T\text{”}\downarrow\text{“Sn”)“+”“} \quad (3)$$

where γ_1 is the gyromagnetic ratio of protons in water, μ the magnetic moment of particles, N_A Avogadro's number, [M] the molarity of particles, r the radius of particle, D the relative diffusive motion of particles, ω_s and ω_t Larmor angular precession frequencies of the NP electric moment and water-proton magnetic moment, respectively, and j_n, (n=1, 2) spectral density functions.[28] In Equation 3, $j_n(\omega, \tau, \tau_{Sn})$ represents spectral density functions, R_e the real part of the expression that follows in parentheses, $\tau(\tau=r^2/D)$ the time scale of fluctuations in the particle–water proton magnetic dipolar interaction arising from the relative diffusive motion of a particle with respect to water molecules, and τ_{Sn} (n=1, 2) are lifetimes of the longitudinal and transverse components of μ, respectively.[28,32]

Fe_3O_4 NPs are a typical example of a contrast-enhanced agent for T_2-weighted imaging. On the basis of a quantum-mechanical outer-sphere theory, the T_2 relaxivity of Fe_3O_4 NPs in solution can be given by:

$$R_2 = \frac{1}{T_2}\left(\frac{256\pi^2\gamma^2}{405}\right)V^*M_s^2\alpha^2/D\,(1 + L/\alpha) \quad (4)$$

where γ is the gyromagnetic ratio of protons, V^* volume fraction, M_s saturation magnetization, α the radius of iron oxide core, D the diffusivity of water molecules, and L the thickness of an impermeable surface coating.[31]

Considering that M_s is the maximum induced magnetic moment obtained in the magnetic field, R_2 is strongly related to γ, coating materials, and the magnetization of NPs is dependent on size, composition, and magnetocrystalline phase, referring to Equations 2–4.[31,33,34] Efforts to improve the efficiency of T_2 agents can be generally rooted in nanocrystal size and composition[34] and hydrodynamic size.[35–37] Compared to traditional colloidal T_2 agents, such as Feridex, Combidex, and Resovist, emerging superparamagnetic oxide NPs with high crystallinity, uniform size, and excellent morphology can generate higher magnetization and further greater T_2-reducing capability. On the other hand, while superparamagnetic NPs are gathered together into small clusters, R_2 can also be improved immensely.[35,36,38] R_2 is proportional to the size of the nanocluster, although the exact reason behind this phenomenon is still unclear.[35] Therefore, the regulation of magnetic nanocrystals' self-assembly may become another available approach to enhance contrast effect greatly in T_1-weighted imaging.

MRI-combined chemotherapy

Although limited in efficacy, cancer chemotherapy has remained one of the most common treatment modalities for many malignant tumors since the early 1950s.[5–7,39] In the case of most anticancer drugs, the lack of specificity toward malignant tissues tends to present a large volume of distribution and then cause significant toxicity and side effects, along with poor solubility in body fluid or blood. Moreover, their low molecular weight makes them easy to be rapidly cleared from the circulation for intravenous administration and not to accumulate well at the pathological site.[5,6] Therefore, in order to develop cancer therapy, two important approaches must be addressed: developing novel probes with high accuracy and precision for early diagnosis, and further enhancing pharmacological specificity or targeting during drug metabolism.[7] Nowadays, multifunctionalized drug-delivery systems have made the integration of MRI and chemotherapy into one "device" come true.

T_1 agents

As described earlier, Gd^{3+} is the metal center of the most common T_1 agents, and many studies on nanocarriers loading Gd and anticancer drugs as T_1-enhanced contrast agents have been reported recently. Vinh et al[40] prepared MRI-detectable polymeric micelles containing Gd-diethylenetriaminepentaacetic acid (DTPA) and the platinum anticancer drug dichloro(1,2-diaminocyclohexane)platinum(II) (DACHPt). The longitudinal T_1 relaxivity (r_1) of Gd-DTPA/DACHPt-loaded micelles greatly increased to 80.7 $mmol \cdot L^{-1} \cdot s^{-1}$, which provided strong and specific tumor-contrast enhancement of T_1-weighted MRI in N1S1 tumor-bearing Sprague Dawley rats. Not only that, this micelle induced high levels (92.4%±3.4%) of tumor apoptosis at 3 days postinjection, but also tumor size and growth in vivo were significantly suppressed without severe adverse reactions (Figure 5).

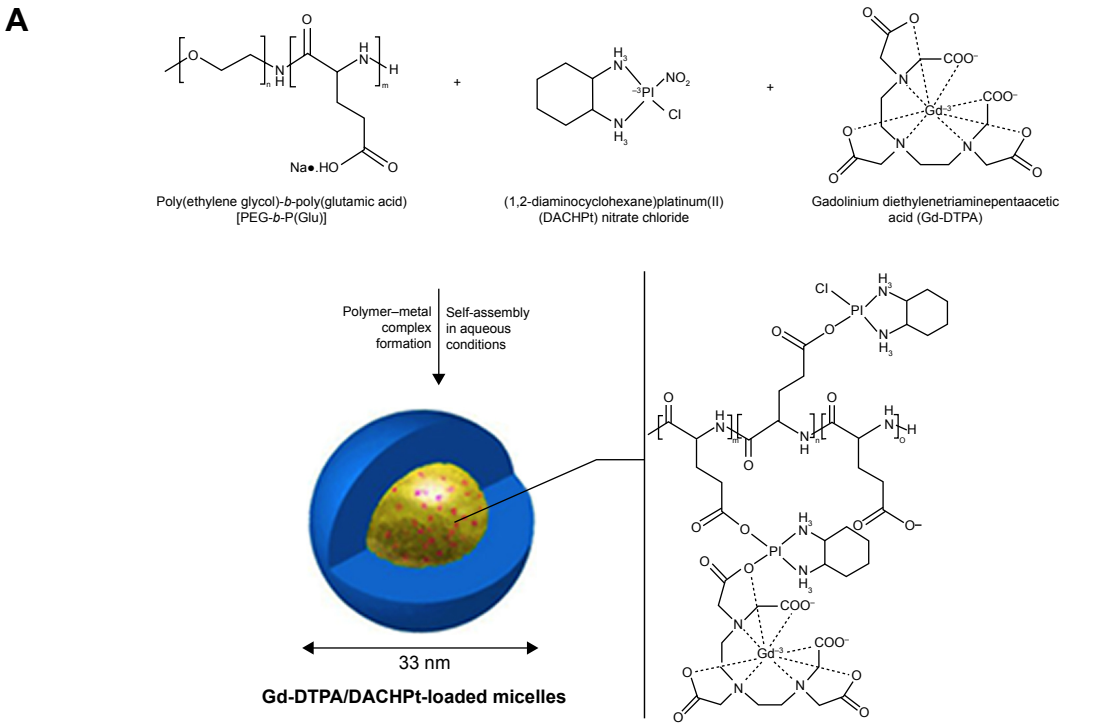

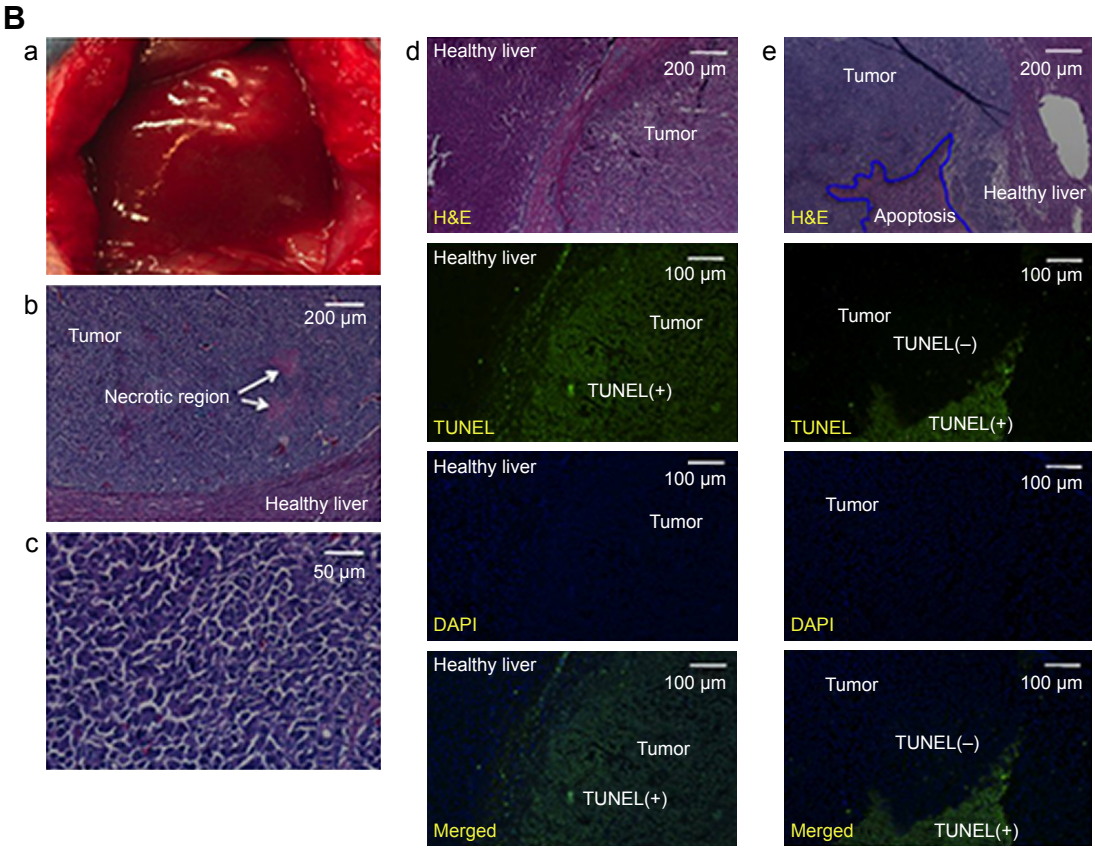

Figure 5 (**A**) Preparation of Gd-DTPA/DACHPt-loaded micelles by self-assembly. (**B**) Tumors, histopathology, and tumor apoptosis. Macroscopic images of an N1S1 hepatic tumor (a–c). Microscopic analysis of H&E-stained tumor sections (showed high levels of tumor apoptosis) and observations from TUNEL, DAPI, and merged images (d, e).

Note: Reprinted from Vinh NQ, Naka S, Cabral H, et al. MRI-detectable polymeric micelles incorporating platinum anticancer drugs enhance survival in an advanced hepatocellular carcinoma model. *Int J Nanomedicine.* 2015;10:4137–4147.[40] Copyright 2015. Dove Medical Press.

Abbreviations: Gd, gadolinium; DTPA, diethylenetriaminepentaacetic acid; DACHPt, dichloro(1,2-diaminocyclohexane)platinum(II); TUNEL, terminal deoxynucleotidyl transferase deoxyuridine triphosphate nick-end labeling; DAPI, 4′,6-diamidino-2-phenylindole.

Likewise, Ma et al[41] constructed renal-clearable NPs consisting of Gd-DTPA and the water-insoluble anticancer drug camptothecin for MRI and chemotherapy. Its r_1 of 4.66 $mM^{-1}\cdot s^{-1}$ showed significant positive contrast enhancement in nude mice bearing LoVo tumors. Slightly different to this nanosystem, Tong et al[42] developed a functionalized polymer of 1,4,7,10-tetraazacyclododecane-1,4,7,10-tetraacetic acid–polyethylene glycol (PEG)-*block*-polyacrylamide-*co*-acrylonitrile to form temperature-responsive micelles coloading doxorubicin (Dox) and Gd ions (Gd^{3+}). The micelles exhibited noticeable accelerated Dox release along with rising temperature, and enhanced MRI in BEL7402 cells with high proton relaxivity (25.88 $mM^{-1}\cdot s^{-1}$).

Both magnetic manganese oxide (MnO_2) and manganese ions are another category of common T_1 agents, and have been studied deeply. For example, Abbasi et al[43] prepared polymeric theranostic NPs encapsulating docetaxel (Dtx), fluorescent dye, and MnO_2 NPs. The novel polymeric theranostic NPs not only sustained in vitro release of Dtx, enhanced energy-dependent cellular uptake, and extended cytoplasmic retention in MDA-MB-231 cells but also enhanced r_1 (2.4 $mM^{-1}\cdot s^{-1}$) to achieve contrast enhancement of T_1-weighted images in a xenograft orthotopic human breast-tumor model. Similarly, Hao et al[44] constructed multifunctional poly(lactic-*co*-glycolic acid) (PLGA) NPs containing hematoporphyrin monomethyl ether and MnO_2 as T_1 agents as well as a drug carrier. Dong et al[45] encapsulated manganese ions with indocyanine green and Dox in theranostic polydopamine NPs with integrated chemotherapy, photothermal therapy (PTT), and MRI. In summary, the theranostic system that combined T_1-weighted MRI and chemotherapy showed positive contrast enhancement and inhibition efficacy on tumor cells simultaneously.

T_2 agents

As the simplest solution, a class of effective theranostic nanoplatforms is developing directly based on the core of MNPs. Asadi et al[46] built pH-sensitive and random copolymer-modified superparamagnetic IONPs (SPIONs) as a promising nanocarrier for MRI and Dox delivery. Both excellent cytocompatibility and cellular uptake in DU145 cells were apparent in this integrated system. It displayed acid-accelerated drug release and MRI-contrast enhancement (r_2=134.4 $mM^{-1}\cdot s^{-1}$). Likewise, Liang et al[47] designed functionalized SPION with a shell of PEGylated Dox. The nanocarriers significantly prolonged the half-life of Dox in blood circulation, improved uptake of HT29 cells under the magnetic field, and strengthened the r_2:r_1 ratio and T_2-weighted signals in an in vivo MRI study of rats. Malekzadeh et al[48] developed a multifunctional quercetin-loaded nanosystem with a core of SPIONs developed through layer-by-layer self-assembly of poly(citric acid) dendrimer, PEG, and folic acid. The total release time of quercetin was prolonged, and excellent cellular uptake and cytotoxicity to HeLa cells and MDA cells were very evident. Of course, the nanovector also led to appreciable negative contrast enhancement in T_2-weighted MRI.

Feng et al[49] chose hollow, mesoporous, Dox-loaded, SPION-entrapped, PEGylated copper sulfide (CuS) NPs to construct smart controllable on-demand cargo delivery (Figure 6). The metal nanohybrid possessed elevated photothermal conversion efficiency (42.12%) for enhanced PTT effect and controlled on-demand drug release upon exposure to a near-infrared (NIR) stimulus for high tumor cytotoxicity. Both in vitro and in vivo experiments revealed remarkable antitumor therapeutic efficacy with the synergistic combination of MRI, photodynamic therapy, PTT, and chemotherapy under NIR irradiation. Similarly, Ren et al[50] constructed a novel paclitaxel-loaded nanocomposite that encapsulated cysteine-functionalized SPIONs, CuS, and paclitaxel into BSA aggregation. These nanoagents can not only absorbed NIR light and transformed it into heat effectively to trigger drug release within the tumor site but also brought sharp T_2-weighted contrast enhancement on a HeLa tumor-bearing mouse. Moreover, An et al[51] utilized glycopolymer-modified magnetic mesoporous silica NPs for liver cancer treatment. The significant recognition ability of HepG2 cells for this nanocarrier greatly facilitated intracellular uptake, controlled drug release, HepG2-cell cytotoxicity, and the contrast effect of T_2-weighted MRI in livers of nude mice.

More often, all kinds of polymeric self-assemblies are chosen as appropriate delivery system for MNPs and antitumor drugs. Du et al[52] constructed temperature-sensitive, folate-targeted, Dtx-loaded magnetic PEGylated liposomes containing fullerene (C_{60})-decorated and PEGylated SPIONs. The multifunctional liposomes achieved the integration of MRI, photothermal tumor ablation, and fullerene radiofrequency-triggered drug release. In vitro and in vivo experiments indicated its high stability, temperature-adjusted release rate, and resulting high efficiency of inhibition on MCF7 cells under 13.56 MHz radiofrequency. In addition, these liposomes gave much brighter T_2-weighted images in female C57 mice bearing B16F10 tumors (Figure 7). In the same way, Wang et al[53] reported on reduction-responsive PEGylated lipid vesicles coloading SPIONs and Dox. The release rate of Dox from these novel vesicles was up to 68.9%

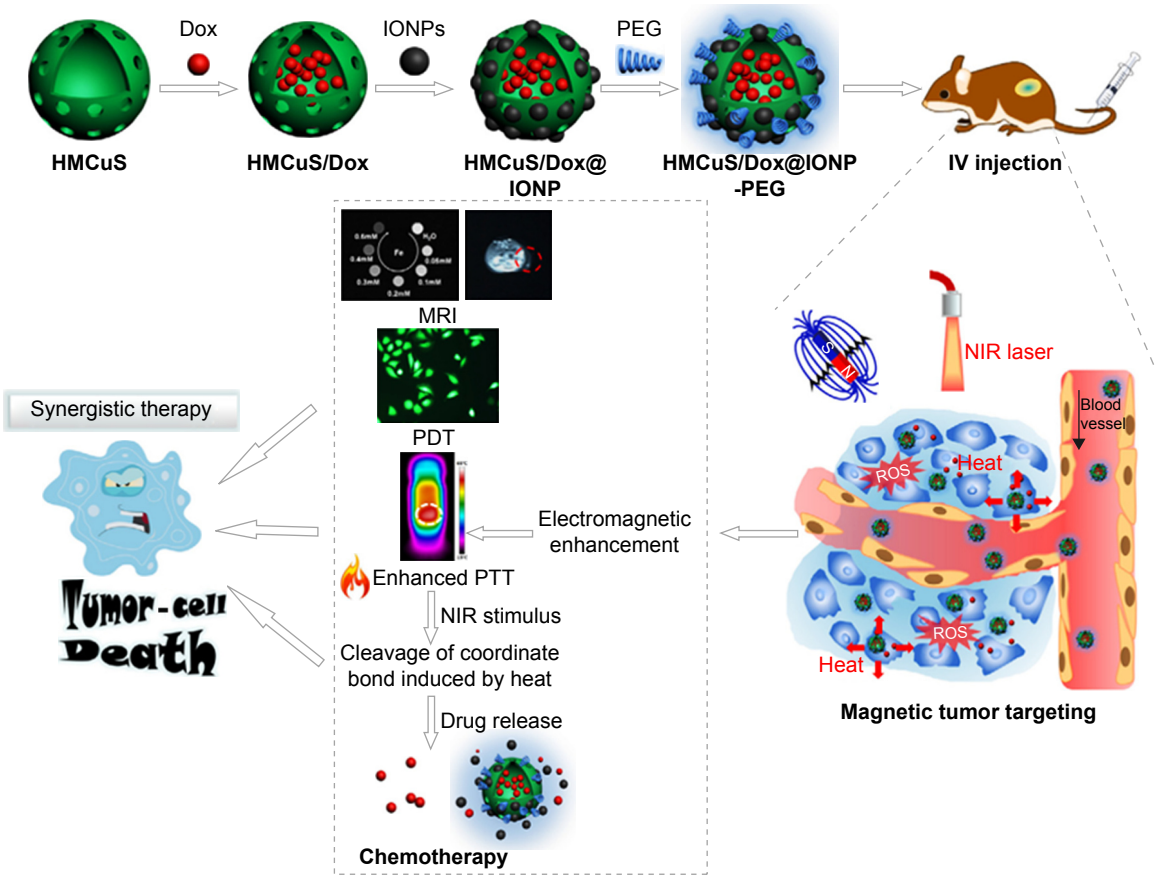

Figure 6 Synthesis of the drug-delivery system (HMCuS/Dox@IONP-PEG) for combining MRI with chemophototherapy.
Note: Reprinted from *Acta Biomater*, 49, Feng Q, Zhang Y, Zhang W, et al, Programmed near-infrared light-responsive drug delivery system for combined magnetic tumor-targeting magnetic resonance imaging and chemo-phototherapy, 402–413.[49] Copyright 2017, with permission from Elsevier.
Abbreviations: Dox, doxorubicin; HM, hollow mesoporous; NPs, nanoparticles; IO, iron oxide; NIR, near-infrared; PTT, phototherapy; PDT, photodynamic therapy; PEG, polyethylene glycol; IV, intravenous; ROS, reactive oxygen species.

in 36 hours in the reduction environment. Cellular uptake, antitumor effect (IC_{50}=1.39 μg·mL^{-1}), and T_2-weighted MRI capability toward HeLa cells were enhanced significantly. Other reduction-sensitive theranostic nanocarriers based on amphiphilic disulfide-linked dextran-*g*-poly(*N*-ω-carbobenzyloxy-L-lysine) (Dex-g-SS-PZLL) were studied by Yang et al.[54] Dox–SPION-coloaded Dex-*g*-SS-PZLL micelles also exhibited reduction-sensitive properties and led to rapid Dox release, higher toxicity to HepG2 cancer cells, and high MRI T_2-weighted imaging sensitivity (r_2=261.3 mM^{-1}·s^{-1}).

Li et al[55] further developed folate-conjugated and PEGylated PLGA NPs with a loaded anticancer drug (sorafenib) and SPIONs for liver cancer therapeutics. This nanocarrier also exhibited sustained drug release, enhanced cellular uptake in cancer cells, effectively suppressed tumor-cell proliferation, and enhanced MRI efficiency. They also studied the colony-forming ability of BEL7402 cells to confirm superior antitumor efficacy. Mosafer et al[56] also applied PLGA NPs as the framework to develop AS1411 aptamer-targeted nanoassemblies coloading SPIONs and Dox against murine C26 colon carcinoma cells. This nanoplatform had slow Dox release over 20 days and prominent cellular uptake and cytotoxicity. These characteristics contributed to improved anti-colon cancer efficacy and contrast effect of T_2-weighted MRI in vivo. Jaidev et al[57] prepared multifunctional PLGA nanospheres containing fluorescent SPIONs and gemcitabine with a surface bonded with HER2 antibody for pancreatic cancer therapy and imaging. Apparently, this theranostic nanosystem achieved sustained release of gemcitabine for 11 days, great inhibition of tumor cells, and significant tumor regression (86%±3%) in male severe combined immunodeficient mice. Moreover, high r_2 relaxivity (773 mM^{-1}·s^{-1}) and a specific absorption rate (183 W·g^{-1}) were determined, which are beneficial to MRI-contrast enhancement and thermotherapy, respectively.

Situ et al[58] synthesized A54 peptide-functionalized PLGA-grafted dextran (A54-DexPLGA) for the formation of A54 homing peptide-functionalized micelles with Dox and SPIONs. The micelles revealed good sustained release and MRI-contrast enhancement similarly to other

nanocarriers. Distinctively, specific targeting to BEL7402 cells caused greater antitumor activity in BEL7402 cells (IC_{50}=0.56 μg mL^{-1}) and tumor-inhibition rate of micelle treatments (72.53%) in orthotopic implantation hepatoma models. Lin et al[59] also studied a multifunctional nanocomposite based on stearic acid chain-grafted amphiphilic dextran (Dex-*g*-SA) and carbohydrate and manganese-doped IONPs (Mn-SPIONs) for Dox delivery and MRI. The Mn-SPION-Dox-loaded Dex-*g*-SA micelles showed low IC_{50} of 1.2 μmol·L^{-1} against MCF7 cells and 15 μmol·L^{-1} against MCF-7/Adr cells. Naturally, it also had good uptake of MCF7/Adr cells and obvious MRI-signal darkening under clinical 3T MRI scanning.

A rather more complex case is multiside groups or multiblock polymers being employed as framework materials. Du et al[60] developed *N*-succinyl-*N*′-4-(2-nitrobenzyloxy)-succinyl-chitosan micelles loading C_{60}, SPIONs, Dtx and upconversion nanophosphors. The micelles regulated controlled drug release on demand by NIR light to improve photodynamic therapy and ROS generation in tumor cells effectively for tumor inhibition. Meanwhile, this novel nanocomposite was also employed for noninvasive deep MRI and upconversion fluorescence imaging. Another example is a multifunctional PEG-PCL nanocarrier with encapsulated SPIONs and busulfan.[61] The theranostic NPs showed sustained drug release over 10 hours and great contrast enhancement

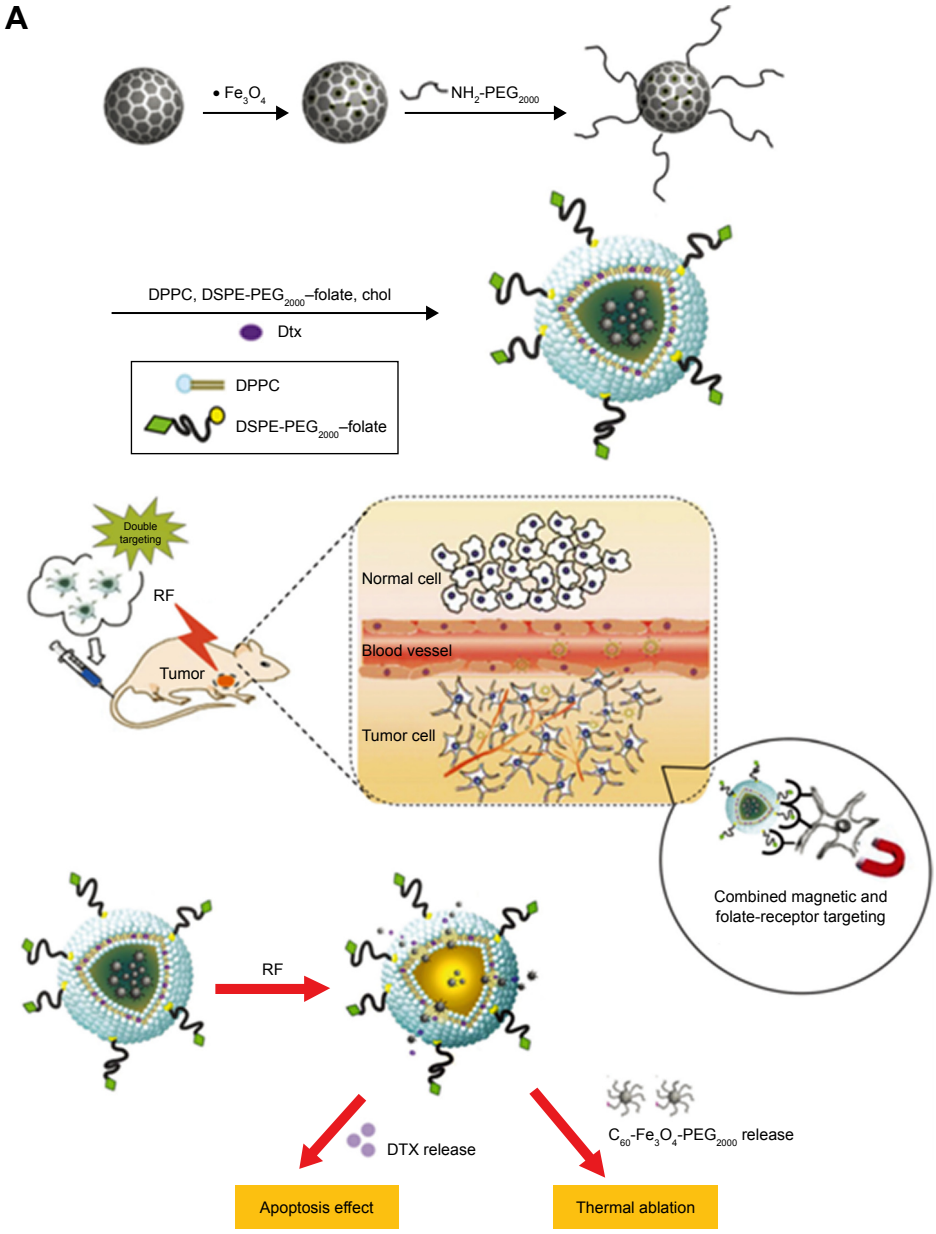

Figure 7 (*Continued*)

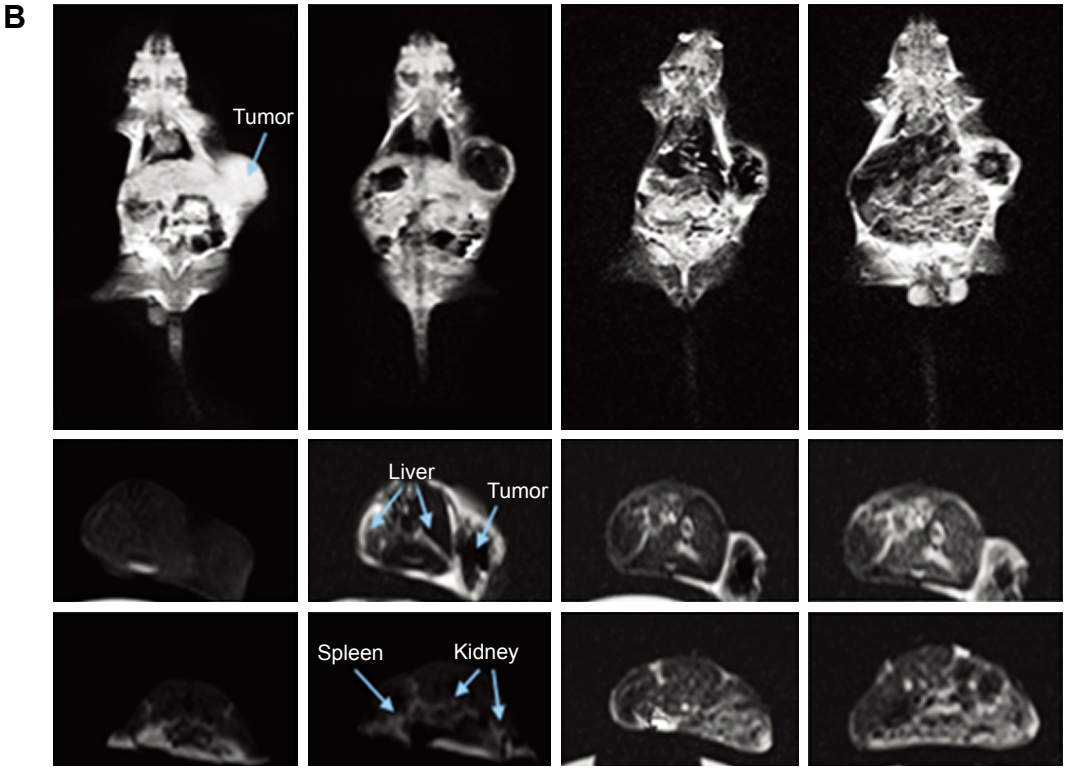

Figure 7 (**A**) Design of functional liposomes with RF-triggered drug release and RF targeted thermochemotherapy using the nanocomposite. (**B**) In vivo T_2-weighted magnetic resonance imaging of multifunctional liposomes with a magnet (left to right: control group and at 1, 4, and 7 hours after injection, respectively).
Note: Reproduced from Du B, Han S, Li H, et al. Multi-functional liposomes showing radiofrequency-triggered release and magnetic resonance imaging for tumor multi-mechanism therapy. *Nanoscale.* 2015;7:5411–5426.[52] Copyright 2015, with permission from the Royal Society of Chemistry.
Abbreviations: Dtx, docetaxel; IONPs, iron oxide nanoparticles; C_{60}, fullerene; PEG, polyethylene glycol; DPPC, dipalmitoylphosphatidylcholine; DSPE, distearoylphosphatidylethanolamine; RF, radiofrequency.

in T_2-weighted MRI with high r_2 (103.3 Fe $mM^{-1}{\cdot}s^{-1}$). In addition, VivoTag 680XL fluorochrome was also labeled to the nanocarriers to observe dynamic biodistribution in vivo and uptake in different organs by fluorescence imaging in real time. Similarly, Lee et al[62] proposed a multifunctional theranostic micelle of cationic PDMA-*b*-PCL and PEG-PCL for loading 7-ethyl-10-hydroxycamptothecin (SN38), ultrasmall SPIONs, and siRNA. This micellar system improved the biostability of the loaded drug and siRNA, prolonged drug release and circulation time, and provided effective T_2-weighted MRI capability. Furthermore, it also efficiently silenced VEGF expression in tumor cells.

More complex and advanced magnetite NPs have also been wrapped inside polymeric nanosystems, such as magnetite nanoclusters (MNCs). Wu et al[63] designed a charge-switchable nanohybrid (HNP-DA) comprising of MNCs, a paclitaxel-loaded core of amphiphilic polymer (pluronic F127), and a hydrophilic polymeric shell of stearoyl-polyethylenimine-2,3-dimethylmalefic anhydride. The surface charge conversion of HNP-DA from negative to positive obviously enhanced uptake efficiency in cancer cells. In vitro studies of HepG2 cells demonstrated that this nanocarrier exhibited very high cytotoxicity at pH 6.5 (<15% cell viability). In addition, the r_2 of the HNP-DA was improved to 142.68 $mM^{-1}{\cdot}s^{-1}$. Likewise, Hayashi et al[64] synthesized folic acid and PEG-decorated NPs with a core of MNCs and shell of Dox-containing polymers. These core–shells realized controlled Dox release for continuous chemotherapy over a long time and enhanced r_2 to 357 $mM^{-1}{\cdot}s^{-1}$. Further under alternating a magnetic field, the core–shells induced heat generation to accelerate drug release within the tumors for outstanding therapeutic efficacy (Figure 8).

Compared with SPIONs, ferric oxide NPs (γ-Fe_2O_3) are another common superparamagnetic T_2-weighted contrast agent. For example, Wang et al[65] developed an innovative tumor-specific multifunctional nanoplatform comprising γ-Fe_2O_3 core and chitosan shell modified with tumor-specific ligand transferrin for anti-tumor theranostics. Thorat et al[66] encapsulated γ-Fe_2O_3 developed together with Dox into *bis*(*p*-sulfonatophenyl)phenylphosphine–methoxypolyethylene glycol–thiol vesicles for consideration of both controlled drug release and enhanced MRI contrast. All results were positive, testifying that this nanocarrier could be also used for synergetic magnetochemotherapy. IONPs, the central

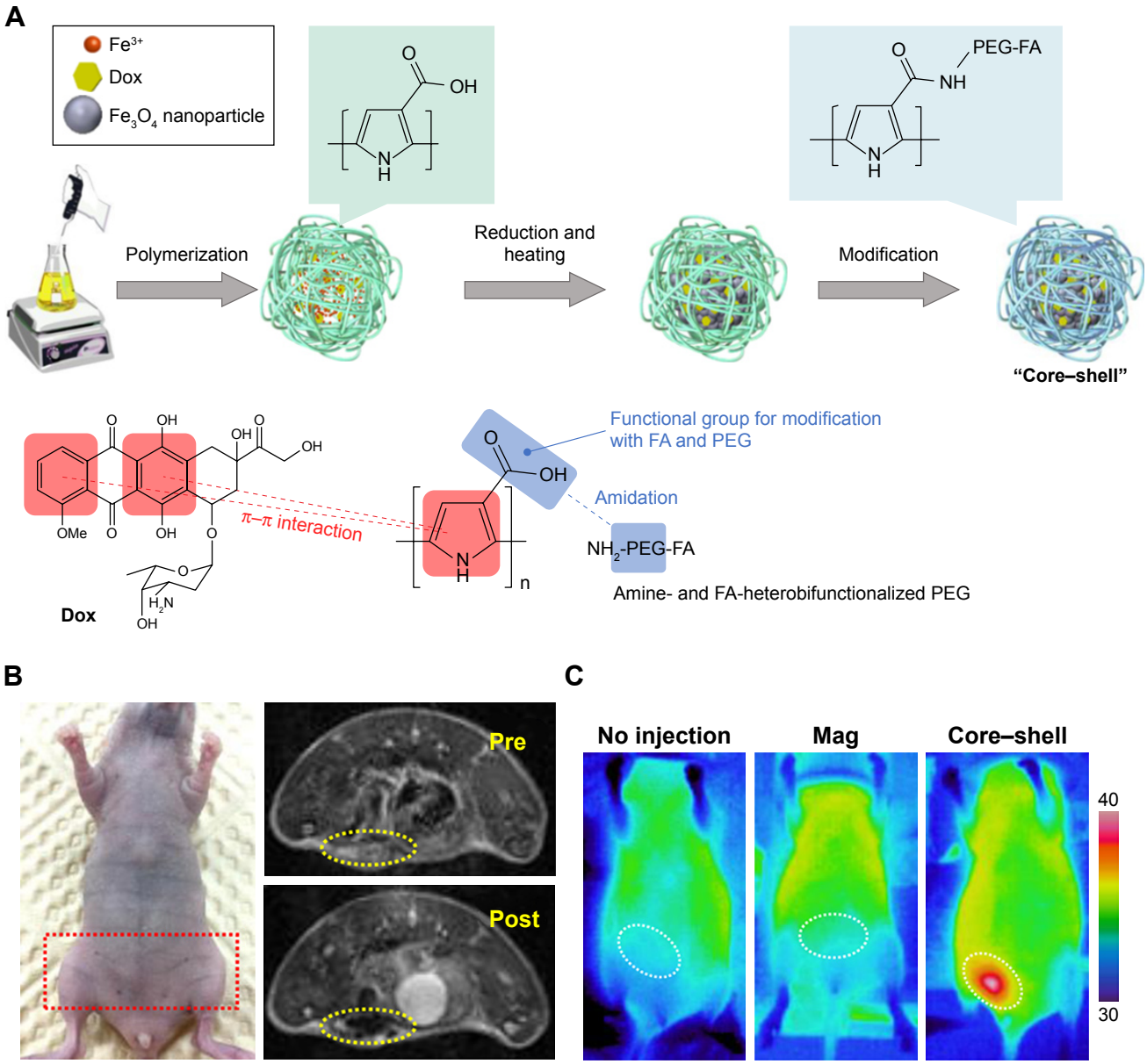

Figure 8 (**A**) Synthesis of magnetic resonance imaging-guided magnetic thermochemotherapy core–shell agents. (**B**) Photography and T_2-weighted magnetic resonance imaging of mice subjected to core–shell injection. (**C**) Thermal images of mice with and without magnetic field or core–shell injection under influence of atomic force microscopy (AMF). The white circles indicate abdominal tumor sites.

Note: Reprinted from Hayashi K, Sato Y, Sakamoto W, Yogo T. Theranostic nanoparticles for MRI-guided thermochemotherapy: "tight" clustering of magnetic nanoparticles boosts relaxivity and heat-generation power. *ACS Biomater Sci Eng*. 2017;3:95–105.[64] Copyright 2017, with permission from the American Chemical Society.

Abbreviations: Dox, doxorubicin; PEG, polyethylene glycol; FA, folic acid; Mag, magnetic.

moiety of the most common T_2 agents, were studied mostly. Others, like γ-Fe_2O_3, magnetic mesoporous silica NPs, and magnetite nanoclusters, were also mentioned as the central moiety. These theranostic systems exhibited excellent negative contrast enhancement in T_2-weighted MRI on account of the loading of T_2-weighted central moieties, and revealed better results for drug delivery and antitumor efficacy.

MRI-combined gene therapy

Gene therapy that involves the delivery of therapeutic genetic material into specific target cells is regarded as a new medical approach for the treatment of tumors. In 1991, the first clinical trial of cancer gene therapy was performed in melanoma patients. To date, most strategies for cancer gene therapy can be classified into five main categories: suicide-gene therapy, rehabilitation of aberrant cell cycle, immunomodulatory gene therapy, antiangiogenesis gene therapy, and oncolytic gene therapy.[67–69]

Among many nonviral gene vectors, polyethylenimine (PEI) is one of the most effective gene-delivery vehicles studied to date. Owing to high charge density, it can effectively bind genes or oligonucleotides to form stable complexes

that can be swallowed easily by cells and escape from intracellular organelles (eg, endosomes) through the proton-sponge effect.[70] Generally, 25 kDa branched PEI and 22 kDa linear PEI are applied as golden standards to evaluate nonviral transfection agents.[71] The presence of primary and secondary amine groups within PEI branches also facilitates various chemical modifications for enhanced functionality.[72] Hydrophobic moieties incorporated into gene-delivery systems are believed to enhance overall cell interactions and tissue permeability.

A new kind of Gd-chelated cationic poly(urethane amide) copolymer (GdCPUAs) was investigated for gene delivery and T_1-weighted MRI by Gao et al.[73] As shown in Figure 9, the Gd-chelated and plasmid DNA-loaded polyplexes showed very high transfection efficiency in different cancer cells and significant T_1-contrast enhancement in vitro (r_1=11.8 $mM^{-1}\cdot s^{-1}$). All the results testified to great potential of biodegradable Gd-chelated cationic poly(urethane amide) copolymers for tumor theranostics. A theranostic micellar delivery system for synergetic gene therapy and T_2-weighted MRI was presented.[60] Park et al[74] integrated multimodal imaging (MRI and Raman imaging) with combined hyperthermia and siRNA-based therapy in multifunctional MNPs with an iron cobalt core and graphitic carbon shell. This system exhibited a higher relaxivity coefficient (r_2=392 $mM^{-1}\cdot s^{-1}$) and delivered small interfering RNA (siRNA) to tumor cells in targeted fashion together with hyperthermia therapy.

MRI-combined thermotherapy

As previously mentioned, the combination of early diagnosis and precise treatment is ideal for cancer therapy, especially represented by thermotherapeutic NPs.[75]

T_1 agents

T_1 agents with metal centers of Gd or Mn have also been combined with thermotherapy for cancer MRI imaging and treatment. Cao et al[76] chose Gd (III)-chelated silica nanospheres ($Gd@SiO_2$) as the framework to integrate Dox and indocyanine green, and then introduced poly (diallyldimethylammonium chloride) to the surface of the magnetic core, as shown in Figure 10. In vitro results revealed that Dox release accelerated significantly at pH 5 or upon NIR irradiation. This was attributed to heat weakening in the electrostatic interactions between Dox and the surface of MNPs. Meanwhile, under laser irradiation, NPs improved therapeutic efficacy by their energy conversion from light to heat. Mi et al[77] developed PEG-*b*-polyanion micelles hybridized with calcium phosphate and Gd-DTPA for imaging-guided Gd neutron-capture tumor therapy. The micelles possessed high molecular relaxivity (18.4 $mM^{-1}\cdot s^{-1}$), suitable for T_1-weighted MRI, and high fatality rate to murine colon adenocarcinoma (C26) cells under thermal neutron irradiation for significantly enhanced therapeutic effects. In addition, tumor growth was effectively suppressed after thermal neutron irradiation. With enhancement of MRI and high energy conversion, these systems not only can be used for T_1-weighted MRI and thermal ablation therapy but also can aggregate with chemotherapy to improve the controlled-release ability of nanocarriers.

T_2 agents

The integration of thermotherapy and MRI into a multifunctional nanoassembly has been achieved.[49,50,52,60,64,78] Also, Chen et al[79] reported PEG-coated NPs with a core of gold NPs and a shell of ferric sulfide for combination of PTT and radiotherapy. In in vitro experiments, the cellular viability of 4T1 cancer cells was greatly inhibited after NP treatment and NIR irradiation. Under the synergistic action of thermoradiotherapy, these NPs significantly induced cell growth and death. Not only that, they also had high r_2 of 213.84 $mM^{-1}\cdot s^{-1}$, which was available for both in vitro and in vivo tumor MRI. Shah et al[80] also developed a magnetic core–shell NP-mediated delivery system for mitochondria-targeting proapoptotic amphipathic tail-anchoring peptide to malignant brain and metastatic breast cancer cells. This system not only can afford noninvasive MRI, but also significantly enhanced the efficacy of the peptide, due to the introduction of magnetic core–shell NP-mediated hyperthermia.

Additionally, dual-modal imaging, multimodal imaging combining thermotherapy, eg, T_1–T_2 dual-modal MRI and MRI–computed tomography (CT)–upconversion luminescence (UCL) multimodal imaging, have also been studied for cancer theranostics. The dysprosium ion (Dy^{3+}) was researched deeply by Liu et al, due to the relatively large K-edge value and highest magnetic moment with the shortest electronic relaxation time of Dy^{3+}. They designed an $NaDyF_4$:50% Lu@Prussian blue nanocomposite for T_1–T_2-weighted MRI, CT, and PTT with the help of the Prussian blue shell.[81] They also developed a UCL-T_2 dual-modal contrast agent with $NaLuF_4$:Yb, Tm/$NaLuF_4$/$NaDyF_4$[82] and a lanthanide-based core−shell−shell nanocomposite $NaYbF_4$:Tm@CaF_2@$NaDyF_4$ for upconversion MRI/CT multimodal imaging.[83] Liu et al[84] developed an Mn_3O_4 contrast agent capped with EDTA and BSA for efficient T_1–T_2 dual-modal imaging and PTT. They also reported an NIR second-window downconversion luminescence and T_2 MRI-contrast agent based on ultrasmall Nd-doped $NaDyF_4$.[85] These studies developed and optimized multifunctional materials for cancer theranostics and went into depth on the

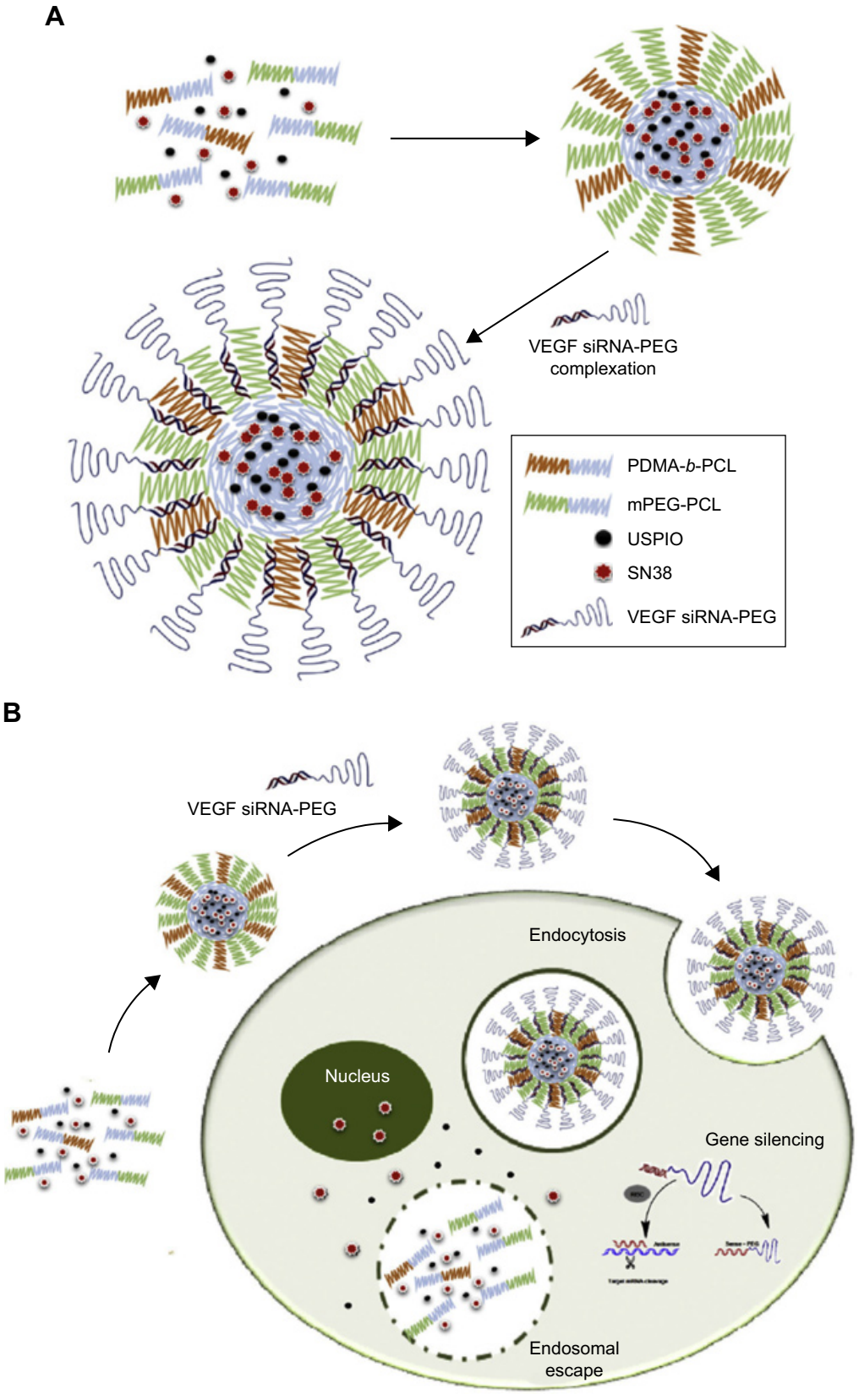

Figure 9 (**A**) Design of multifunctional SN38/USPIO-loaded siRNA-PEG micelle complexes. (**B**) Synthesis process and intracellular therapeutic mechanism of multifunctional SN38/USPIO-loaded siRNA-PEG micelle complexes.

Note: Reprinted from *Biomaterials*, 86, Lee SY, Yang CY, Peng CL, et al, A theranostic micelleplex Co-delivering Sn-38 and VEGF siRNA for colorectal cancer therapy, 92–105.[62] Copyright 2016, with permission from Elsevier.

Abbreviations: PDMA, poly(2-[dimethylamino]ethyl methacrylate); PCL, polycaprolactone; SN38, 7-ethyl-10-hydroxycamptonthecin; USPIO, ultrasmall superparamagnetic iron oxide; PEG, polyethylene glycol.

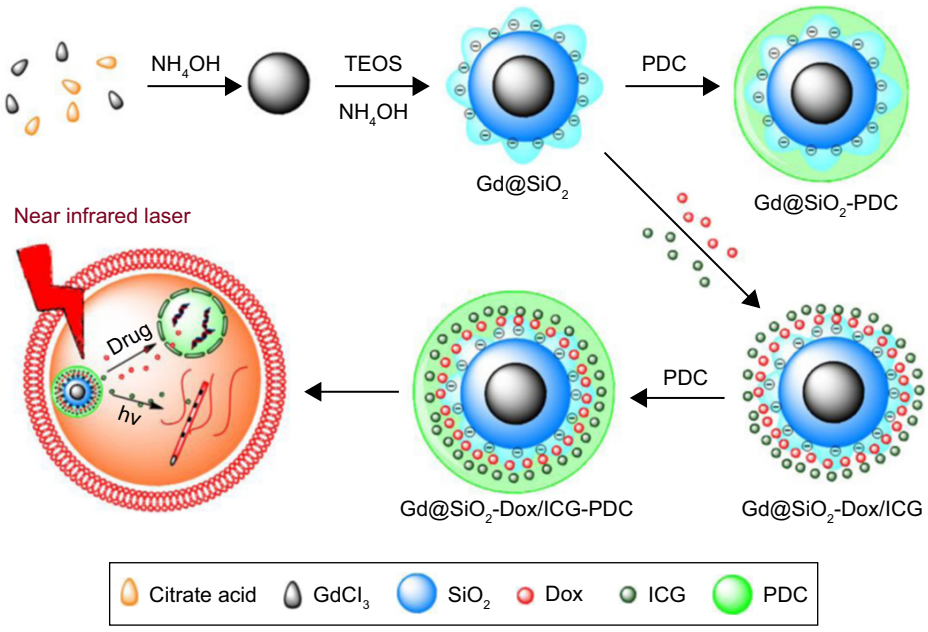

Figure 10 Synthesis of Gd@SiO_2-PDC and Gd@SiO_2-Dox/ICG-PDC.
Notes: Reprinted with permisison from Cao M, Wang P, Kou Y, et al. Gadolinium (III)-chelated silica nanospheres integrating chemotherapy and photothermal therapy for cancer treatment and magnetic resonance imaging. *ACS Appl Mater Interfaces.* 2015;7:25014–25023.[76] Copyright 2015, American Chemical Society.
Abbreviations: Gd, gadolinium; Dox, doxorubicin; ICG, indocyanine green; PDC, polydiallyldimethylammonium chloride; TEOS, tetraethyl orthosilicate.

feasibility of multimodal imaging for cancer theranostics and imaging-guided PTT.

Magnetic fluid hyperthermia[86] is also a superior method of thermotherapy used for cancer therapy, and is based on the property of the contrast agents within the magnetic field. Thorat et al[87] functionalized superparamagnetic $La_{0.7}Sr_{0.3}MnO_3$ NPs with an oleic acid–PEG–polymeric micelle structure and loaded it with Dox. The design combined the effects of magnetic hyperthermia produced by particles under MRI and controlled drug release, and showed that cancer-cell killing was up to almost 90%. Other polymer-coated MNPs were studied by Boni et al.[88] They synthesized MNPs by decomposition of iron pentacarbonyl, growth with iron oleate, and further coating with polyamidoamine. The optimized MNPs (faceted-like) exhibited excellent transverse relaxivity (r_2~300 $mM^{-1}\cdot s^{-1}$) that was 2.5–3 times higher than the commercial Endorem and very high specific loss of power up to 900 $W\cdot g^{-1}$ at 262 kHz and 10 $kA\cdot m^{-1}$. This could be a suitable candidate contrast agent for simultaneous hyperthermic treatment and MRI diagnosis of cancer. In addition, Hatamie et al[89] also designed a novel MRI-contrast agent with graphene–cobalt nanocomposites, which exhibited superior conversion of electromagnetic energy into heat and achieved the integration of MRI and hyperthermia therapy for cancer. Liu et al[90] synthesized ferromagnetic $Fe_{0.6}Mn_{0.4}O$ nanoflowers for T_1–T_2 dual-mode MRI and magnetic hyperthermia therapy. Both in vitro and in vivo results showed excellent magnetic induction-heating effects of the nanoflowers and great therapeutic effect on MCF7 breast cancer. To avoid local overheating, Herynek et al[91] studied novel silica-coated ($La_{1-x}Sr_xMnO_3$) ferromagnetic NPs with low Curie temperature, which induced cell apoptosis and cell death with thermoablation and MRI in cancer cells.

MRI-combined radiotherapy

Despite unavoidable organ exposure and potential cancer risk, radiotherapy is still one of the most effective treatments for malignant tumors.[92] Li et al[93] synthesized PEG-coated Au@MnS@ZnS core–shell–shell NPs for MRI-guided X-ray irradiation, as shown in Figure 11. The results indicated that these NPs enhanced 4T1 cell-killing efficiency and inhibited tumor growth dramatically, owing to severe DNA damage in tumor cells under X-ray irradiation. Paramagnetic Mn^{2+} in the NP shell made these NPs usable as a T_1-weighted MRI contrast agent to guide treatment section precisely for improving therapeutic efficacy. Similarly, Dou et al[94] developed a multifunctional PEG-decorated nanotheranostic with a core of Prussian blue NPs and a bonded satellite of gold NPs for synergistic MRI, CT, PTT, and radiosensitive therapy. These radial NPs combined the properties of both r_1 (7.48 $mM^{-1}\cdot s^{-1}$) and r_2 (8.02 $mM^{-1}\cdot s^{-1}$) values to achieve simultaneous T_1- and T_2-weighted MR contrast. After NIR and X-ray irradiation treatment, <11% of 4T1 cancer cells remained alive in vitro. Tumor growth in vivo was entirely

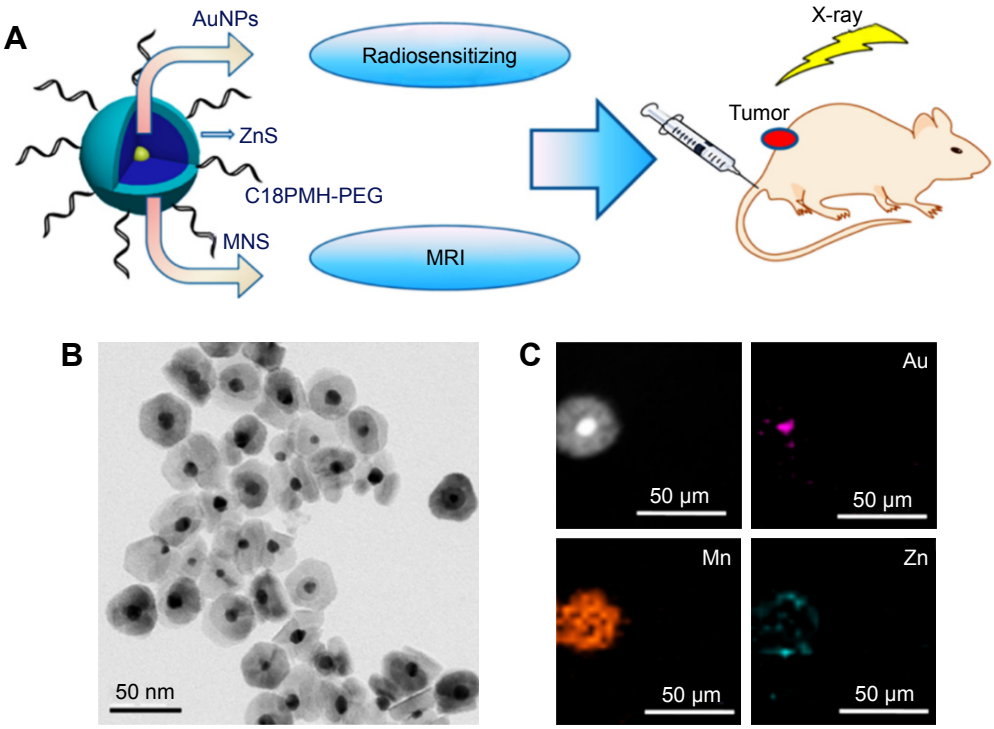

Figure 11 PEG-coated Au@MnS@ZnS core-shell-shell NPs for MRI-guided X-ray irradiation.
Notes: (**A**) Design of Au@MnS@ZnS NPs. (**B**) Transmission electron microscopy of Au@MnS@ZnS NPs. (**C**) Elemental mapping (Au, Mn, and Zn) of an Au@MnS@ZnS NP. According to the parameter of TEM and the rod of the figures, we can know that (**B**) was observed at 400× magnification. (**C**) was observed at 400× magnification. Reprinted with permission from Li M, Zhao Q, Yi X, et al. Au@MnS@ZnS core/shell/shell nanoparticles for magnetic resonance imaging and enhanced cancer radiation therapy. *ACS Appl Mater Interfaces.* 2016;8:9557–9564.[93] Copyright 2016, American Chemical Society.
Abbreviations: AuNPs, gold nanoparticles; C18PMH-PEG, polyethylene glycol-grafted poly(maleic anhydride-*alt*-1-octadecene).

suppressed, and the death of 4T1-xenograft tumor-bearing mice was also remarkably delayed under synergetic treatments. Novel trimodal theranostic NPs consisting of silica nanospheres, polysiloxane shells, and Bi/Gd-DOTA chelate-grafted outside surfaces were prepared by Detappe et al.[95] These NPs showed great MRI- and CT-contrast enhancement in vivo. They also attained outstanding improvement in tumor-growth delay followed by radiation in the subcutaneous xenograft solid-tumor model.

Conclusion

Some problems, including functional integrity, harmony, and mutual promotion, still exist, although cancer-specific theranostic agents or systems have made great progress. In future, several key points may be focused on in the design of more advanced multifunctional devices with enhanced imaging accuracy and therapeutic efficiency for cancer treatment:

(1) MRI contrast agent with high imaging sensitivity. SPIONs' magnetic susceptibility is relevant to their physical/chemical properties (eg, crystal form, size, surface property, aggregation density, and morphology), and Gd complexes depend on local concentration and interaction with water molecules. In addition, some doped rare-metal elements can also greatly improve contrast effects.
(2) Tumor-targeting moiety with high specificity. Currently, specific peptides, antibodies, and aptamers with universal single tumor targeting have been studied. Their high tumor specificity would favor therapeutic agents or systems accumulated effectively within the cancer region.
(3) Appropriate carriers. Besides size, both the morphology and surface properties of delivery systems can affect their stability, drug-release rate, cell uptake, and circulation time in vivo. Substrate material is crucial to achieve low toxicity, high stability, high loading efficiency, and controlled release. Particularly, drug-controlled release best possessed tumor-specific responsiveness due to the conversion from passivity to initiative. Now, amphiphilic, biodegradable, and biocompatible polymers have become the first choice.

Novel magnetic polymer nanoassemblies are constantly emerging, but almost none can enter clinical trials, let them alone improve theranostic effects or decrease costs. It seems only right to find a better solution with appropriate balance between structure and function to develop simple but effective integration for cancer theranostics.

Acknowledgments

This work was financially supported by Guangdong Provincial Key Laboratory of Optical Information Materials and Technology (grant 2017B030301007), the Special Fund on Public Interest Research and Capacity Building in Guangdong Province (2015A020211024), the Natural Science Foundation of China (No. 51773069), the Guangdong Innovative Research Team Program (2013C102), MOE International Laboratory for Optical Information Technologies, and the 111 Project.

Disclosure

The authors report no conflicts of interest in this work.

References

1. Siegel RL, Miller KD, Jemal A. Cancer statistics, 2017. *CA Cancer J Clin*. 2017;67:7–30.
2. Jemal A, Bray F, Center MM, Ferlay J, Ward E, Forman D. Global cancer statistics. *CA Cancer J Clin*. 2011;61:69–90.
3. Funkhouser J. Reinventing pharma: the theranostic revolution. *Curr Drug Discov*. 2002;2:17–19.
4. Kelkar SS, Reineke TM. Theranostics: combining imaging and therapy. *Bioconjug Chem*. 2011;22:1879–1903.
5. Lammers T, Kiessling F, Hennink WE, Storm G. Nanotheranostics and image-guided drug delivery current concepts and future direction. *Mol Pharm*. 2010;7:1899–1912.
6. Xin Y, Huang Q, Tang JQ, et al. Nanoscale drug delivery for targeted chemotherapy. *Cancer Lett*. 2016;379:24–31.
7. Yong KT, Roy I, Swihart MT, Prasad PN. Multifunctional nanoparticles as biocompatible targeted probes for human cancer diagnosis and therapy. *J Mater Chem*. 2009;19:4655–4672.
8. Bharali DJ, Mousa SA. Emerging nanomedicines for early cancer detection and improved treatment: current perspective and future promise. *Pharmacol Ther*. 2010;128:324–335.
9. Ringsdorf H. Structure and properties of pharmacologically active polymers. *J Polym Sci Symp*. 1975;51:135–153.
10. Barreto JA, O'Malley W, Kubeil M, Graham B, Stephan H, Spiccia L. Nanomaterials: applications in cancer imaging and therapy. *Adv Mater*. 2011;23:H18–H40.
11. Hu CM, Zhang L. Nanoparticle-based combination therapy toward overcoming drug resistance in cancer. *Biochem Pharmacol*. 2012;83:1104–1111.
12. Wolinsky JB, Colson YL, Grinstaff MW. Local drug delivery strategies for cancer treatment: gels, nanoparticles, polymeric films, rods, and wafers. *J Control Release*. 2012;159:14–26.
13. Liechty WB, Peppas NA. Expert opinion: responsive polymer nanoparticles in cancer therapy. *Eur J Pharm Biopharm*. 2012;80:241–246.
14. Larson N, Ghandehari H. Polymeric conjugates for drug delivery. *Chem Mater*. 2012;24:840–853.
15. Wankhede M, Bouras A, Kaluzova M, Hadjipanayis CG. Magnetic nanoparticles: an emerging technology for malignant brain tumor imaging and therapy. *Expert Rev Clin Pharmacol*. 2012;5:173–186.
16. Månsson S, Bjørnerud A. Physical principles of medical imaging by nuclear magnetic resonance. In: Tóth E, Merbach AE, editors. *The Chemistry of Contrast Agents in Medical Magnetic Resonance Imaging*. Chichester, UK: Wiley; 2001:1–44.
17. Yan GP, Zhuo RX. Research progress of magnetic resonance imaging contrast agents. *Chin Sci Bulll*. 2001;46:1233–1237.
18. Wei H, Bruns OT, Kaul MG, et al. Exceedingly small iron oxide nanoparticles as positive MRI contrast agents. *Proc Natl Acad Sci U S A*. 2017;114:2325–2330.
19. Khemtong C, Kessinger CW, Gao J. Polymeric nanomedicine for cancer MR imaging and drug delivery. *Chem Commun (Camb)*. 2009:3497–3510.
20. Peng YK, Tsang SC, Chou PT. Chemical design of nanoprobes for T1-weighted magnetic resonance imaging. *Mater Today*. 2016;19:336–348.
21. Yan GP, Robinson L, Hogg P. Magnetic resonance imaging contrast agents: overview and perspectives. *Radiography*. 2007;13:e5–e19.
22. Geraldes CF, Laurent S. Classification and basic properties of contrast agents for magnetic resonance imaging. *Contrast Media Mol Imaging*. 2009;4:1–23.
23. Fass L. Imaging and cancer: a review. *Mol Oncol*. 2008;2:115–152.
24. Bloembergen N, Morgan LO. Proton relaxation times in paramagnetic solutions: effects of electron spin relaxation. *J Chem Phys*. 1961;34:842–850.
25. Caravan P. Strategies for increasing the sensitivity of gadolinium based MRI contrast agents. *Chem Soc Rev*. 2006;35:512–523.
26. Villaraza AJ, Bumb A, Brechbiel MW. Macromolecules, dendrimers, and nanomaterials in magnetic resonance imaging: the interplay between size, function, and pharmacokinetics. *Chem Rev*. 2010;110:2921–2959.
27. Ai H. Layer-by-layer capsules for magnetic resonance imaging and drug delivery. *Adv Drug Deliv Rev*. 2011;63:772–788.
28. Seymour H, Koenig KE. Theory of 1/T1 and 1/T2 NMRD profiles of solutions of magnetic nanoparticles. *Magn Reson Med*. 1995;34:227–233.
29. Rodney A, Brooks FM, Gillis P. On T2-shortening by weakly magnetized particles: the chemical exchange model. *Magn Reson Med*. 2001;45:1014–1020.
30. Gillis P, Moiny F, Brooks RA. On T_2-shortening by strongly magnetized spheres: a partial refocusing model. *Magn Reson Med*. 2002;47:257–263.
31. Tong S, Hou S, Zheng Z, Zhou J, Bao G. Coating optimization of superparamagnetic iron oxide nanoparticles for high T2 relaxivity. *Nano Lett*. 2010;10:4607–4613.
32. Jun YW, Lee JH, Cheon J. Chemical design of nanoparticle probes for high-performance magnetic resonance imaging. *Angew Chem Int Ed Engl*. 2008;47:5122–5135.
33. Sun S, Zeng H, Robinson DB, et al. Monodisperse MFe_2O_4 (M = Fe, Co, Mn) nanoparticles. *J Am Chem Soc*. 2004;126:273–279.
34. Lee JH, Huh YM, Jun YW, et al. Artificially engineered magnetic nanoparticles for ultra-sensitive molecular imaging. *Nat Med*. 2007;13:95–99.
35. Ai H, Brent C, Weinberg B, et al. Magnetite-loaded polymeric micelles as ultrasensitive magnetic-resonance probes. *Adv Mater*. 2005;17:1949–1952.
36. Wang Z, Liu G, Sun J, et al. Self-assembly of magnetite nanocrystals with amphiphilic polyethylenimine: structures and applications in magnetic resonance imaging. *J Nanosci Nanotechnol*. 2009;9:378–385.
37. Liu G, Wang Z, Lu J, et al. Low molecular weight alkyl-polycation wrapped magnetite nanoparticle clusters as MRI probes for stem cell labeling and in vivo imaging. *Biomaterials*. 2011;32:528–537.
38. Lu J, Ma S, Sun J, et al. Manganese ferrite nanoparticle micellar nanocomposites as MRI contrast agent for liver imaging. *Biomaterials*. 2009;30:2919–2928.
39. Wu CP, Hsieh CH, Wu YS. The emergence of drug transporter-mediated multidrug resistance to cancer chemotherapy. *Mol Pharm*. 2011;8:1996–2011.
40. Vinh NQ, Naka S, Cabral H, et al. MRI-detectable polymeric micelles incorporating platinum anticancer drugs enhance survival in an advanced hepatocellular carcinoma model. *Int J Nanomedicine*. 2015;10:4137–4147.
41. Ma Y, Mou Q, Sun M, et al. Cancer theranostic nanoparticles self-assembled from amphiphilic small molecules with equilibrium shift-induced renal clearance. *Theranostics*. 2016;6:1703–1716.
42. Tong G, Fang Z, Huang G, et al. Gadolinium/DOTA functionalized poly(ethylene glycol)-block-poly(acrylamide-co-acrylonitrile) micelles with synergistically enhanced cellular uptake for cancer theranostics. *RSC Adv*. 2016;6:50534–50542.

43. Abbasi AZ, Prasad P, Cai P, et al. Manganese oxide and docetaxel co-loaded fluorescent polymer nanoparticles for dual modal imaging and chemotherapy of breast cancer. *J Control Release*. 2015;209:186–196.
44. Hao Y, Zhang B, Zheng C, et al. Multifunctional nanoplatform for enhanced photodynamic cancer therapy and magnetic resonance imaging. *Colloids Surf B Biointerfaces*. 2017;151:384–393.
45. Dong Z, Gong H, Gao M, et al. Polydopamine nanoparticles as a versatile molecular loading platform to enable imaging-guided cancer combination therapy. *Theranostics*. 2016;6:1031–1042.
46. Asadi H, Khoee S, Deckers R. Polymer-grafted superparamagnetic iron oxide nanoparticles as a potential stable system for magnetic resonance imaging and doxorubicin delivery. *RSC Adv*. 2016;6:83963–83972.
47. Liang PC, Chen YC, Chiang CF, et al. Doxorubicin-modified magnetic nanoparticles as a drug delivery system for magnetic resonance imaging-monitoring magnet-enhancing tumor chemotherapy. *Int J Nanomedicine*. 2016;11:2021–2037.
48. Malekzadeh AM, Ramazani A, Rezaei SJT, Niknejad H. Design and construction of multifunctional hyperbranched polymers coated magnetite nanoparticles for both targeting magnetic resonance imaging and cancer therapy. *J Colloid Interface Sci*. 2017;490:64–73.
49. Feng Q, Zhang Y, Zhang W, et al. Programmed near-infrared light-responsive drug delivery system for combined magnetic tumor-targeting magnetic resonance imaging and chemo-phototherapy. *Acta Biomater*. 2017;49:402–413.
50. Ren L, Liu X, Wang Q, et al. Facile fabrication of a magnetically smart PTX-loaded Cys-Fe_3O_4/CuS@BSA nano-drug for imaging-guided chemo-photothermal therapy. *Dalton Trans*. 2017;46:2204–2213.
51. An J, Zhang X, Guo Q, Zhao Y, Wu Z, Li C. Glycopolymer modified magnetic mesoporous silica nanoparticles for MR imaging and targeted drug delivery. *Colloids Surf A Physicochem Eng Asp*. 2015;482:98–108.
52. Du B, Han S, Li H, et al. Multi-functional liposomes showing radiofrequency-triggered release and magnetic resonance imaging for tumor multi-mechanism therapy. *Nanoscale*. 2015;7:5411–5426.
53. Wang S, Yang W, Du H, et al. Multifunctional reduction-responsive SPIO&DOX-loaded PEGylated polymeric lipid vesicles for magnetic resonance imaging-guided drug delivery. *Nanotechnology*. 2016;27:165101.
54. Yang HK, Qi M, Mo L, et al. Reduction-sensitive amphiphilic dextran derivatives as theranostic nanocarriers for chemotherapy and MR imaging. *RSC Adv*. 2016;6:114519–114531.
55. Li YJ, Dong M, Kong FM, Zhou JP. Folate-decorated anticancer drug and magnetic nanoparticles encapsulated polymeric carrier for liver cancer therapeutics. *Int J Pharm*. 2015;489:83–90.
56. Mosafer J, Abnous K, Tafaghodi M, Mokhtarzadeh A, Ramezani M. In vitro and in vivo evaluation of anti-nucleolin-targeted magnetic PLGA nanoparticles loaded with doxorubicin as a theranostic agent for enhanced targeted cancer imaging and therapy. *Eur J Pharm Biopharm*. 2017;113:60–74.
57. Jaidev LR, Chellappan DR, Bhavsar DV, et al. Multi-functional nanoparticles as theranostic agents for the treatment and imaging of pancreatic cancer. *Acta Biomater*. 2017;49:422–433.
58. Situ JQ, Wang XJ, Zhu XL, et al. Multifunctional SPIO/DOX-loaded A54 homing peptide functionalized dextran-g-PLGA micelles for tumor therapy and MR imaging. *Sci Rep*. 2016;6:35910.
59. Lin B, Su H, Jin R, et al. Multifunctional dextran micelles as drug delivery carriers and magnetic resonance imaging probes. *Sci Bull*. 2015;60:1272–1280.
60. Du B, Han S, Zhao F, et al. A smart upconversion-based light-triggered polymer for synergetic chemo-photodynamic therapy and dual-modal MR/UCL imaging. *Nanomedicine*. 2016;12:2071–2080.
61. Asem H, Zhao Y, Ye F, et al. Biodistribution of biodegradable polymeric nano-carriers loaded with busulphan and designed for multimodal imaging. *J Nanobiotechnol*. 2016;14:82.
62. Lee SY, Yang CY, Peng CL, et al. A theranostic micelleplex Co-delivering Sn-38 and VEGF siRNA for colorectal cancer therapy. *Biomaterials*. 2016;86:92–105.
63. Wu L, Wu M, Lin X, Zhang X, Liu X, Liu J. Magnetite nanocluster and paclitaxel-loaded charge-switchable nanohybrids for MR imaging and chemotherapy. *J Mater Chem B*. 2017;5:849–857.
64. Hayashi K, Sato Y, Sakamoto W, Yogo T. Theranostic nanoparticles for MRI-guided thermochemotherapy: "tight" clustering of magnetic nanoparticles boosts relaxivity and heat-generation power. *ACS Biomater Sci Eng*. 2017;3:95–105.
65. Wang X, Chang Y, Zhang D, Tian B, Yang Y, Wei F. Transferrin-conjugated drug/dye-co-encapsulated magnetic nanocarriers for active-targeting fluorescent/magnetic resonance imaging and anti-tumor effects in human brain tumor cells. *RSC Adv*. 2016;6:105661–105675.
66. Thorat ND, Lemine OM, Bohara RA, Omri K, el Mir L, Tofail SA. Superparamagnetic iron oxide nanocargoes for combined cancer thermotherapy and MRI applications. *Phys Chem Chem Phys*. 2016;18:21331–21339.
67. Kang JH, Toita R, Katayama Y. Bio and nanotechnological strategies for tumor-targeted gene therapy. *Biotechnol Adv*. 2010;28:757–763.
68. Cao S, Cripps A, Wei MQ. New strategies for cancer gene therapy: progress and opportunities. *Clin Exp Pharmacol Physiol*. 2010;37:108–114.
69. Conde J, Arnold CE, Tian F, Artzi N. RNAi nanomaterials targeting immune cells as an anti-tumor therapy: the missing link in cancer treatment. *Mater Today*. 2016;19:29–43.
70. Boussif O, Lezoualc'h F, Zanta MA, et al. A versatile vector for gene and oligonucleotide transfer into cells in culture and in vivo polyethylenimine. *Proc Natl Acad Sci U S A*. 1995;92:7297–7301.
71. Bonetta L. The inside scoop-evaluating gene delivery methods. *Nat Methods*. 2005;2:878–881.
72. Thomas M, Klibanov AM. Enhancing polyethylenimine's delivery of plasmid DNA into mammalian cells. *Proc Natl Acad Sci U S A*. 2002;99:14640–14645.
73. Gao X, Wang G, Shi T, et al. Biodegradable gadolinium-chelated cationic poly(urethane amide) copolymers for gene transfection and magnetic resonance imaging. *Mater Sci Eng C Mater Biol Appl*. 2016;65:181–187.
74. Park JK, Jung J, Subramaniam P, et al. Graphite-coated magnetic nanoparticles as multimodal imaging probes and cooperative therapeutic agents for tumor cells. *Small*. 2011;7:1647–1652.
75. Bayazitoglu Y, Kheradmand S, Tullius TK. An overview of nanoparticle assisted laser therapy. *Int J Heat Mass Transf*. 2013;67:469–486.
76. Cao M, Wang P, Kou Y, et al. Gadolinium (III)-chelated silica nanospheres integrating chemotherapy and photothermal therapy for cancer treatment and magnetic resonance imaging. *ACS Appl Mater Interfaces*. 2015;7:25014–25023.
77. Mi P, Dewi N, Yanagie H, et al. Hybrid calcium phosphate-polymeric micelles incorporating gadolinium chelates for imaging-guided gadolinium neutron capture tumor therapy. *ACS Nano*. 2015;9:5913–5921.
78. Chen Y, Ai K, Liu J, Ren X, Jiang C, Lu L. Polydopamine-based coordination nanocomplex for T1/T2 dual mode magnetic resonance imaging-guided chemo-photothermal synergistic therapy. *Biomaterials*. 2016;77:198–206.
79. Chen J, Li M, Yi X, et al. Synergistic effect of thermo-radiotherapy using Au@FeS core-shell nanoparticles as multifunctional therapeutic nanoagents. *Part Part Syst Charact*. 2017;34:1600330.
80. Shah BP, Pasquale N, De G, Tan T, Ma J, Lee KB. Core-shell nanoparticle-based peptide therapeutics and combined hyperthermia for enhanced cancer cell apoptosis. *ACS Nano*. 2014;8:9379–9387.
81. Liu Y, Guo Q, Zhu X, et al. Optimization of Prussian blue coated $NaDyF_4$:*x*%Lu nanocomposites for multifunctional imaging-guided photothermal therapy. *Adv Funct Mater*. 2016;26:5120–5130.
82. Yuan W, Yang D, Su Q, et al. Intraperitoneal administration of biointerface-camouflaged upconversion nanoparticles for contrast enhanced imaging of pancreatic cancer. *Adv Funct Mater*. 2016;26:8631–8642.

83. Li Y, Gu Y, Yuan W, et al. Core–shell−shell $NaYbF_4$:Tm@CaF_2@$NaDyF_4$ nanocomposites for upconversion/T_2-weighted MRI/computed tomography lymphatic imaging. *ACS Appl Mater Interfaces*. 2016;8:19208−19216.
84. Liu Y, Zhang G, Guo Q, et al. Artificially controlled degradable inorganic nanomaterial for cancer theranostics. *Biomaterials*. 2017;112:204−217.
85. Liu Y, Fan H, Guo Q, Jiang A, Du X, Zhou J. Ultra-small pH-responsive Nd-doped $NaDyF_4$ nanoagents for enhanced cancer theranostic by in situ aggregation. *Theranostics*. 2017;7:4218−4228.
86. Demirer GS, Okurb AC, Kizilel S. Synthesis and design of biologically inspired biocompatible iron oxide nanoparticles for biomedical applications. *J Mater Chem B*. 2015;3:7831−7849.
87. Thorat ND, Bohara RA, Noor MR, Dhamecha D, Soulimane T, Tofail SA. Effective cancer theranostics with polymer encapsulated superparamagnetic nanoparticles: combined effects of magnetic hyperthermia and controlled drug release. *ACS Biomater Sci Eng*. 2017;3:1332−1340.
88. Boni A, Basini AM, Capolupo L, et al. Optimized PAMAM coated magnetic nanoparticles for simultaneous hyperthermic treatment and contrast enhanced MRI diagnosis. *RSC Adv*. 2017;7:44104–44111.
89. Hatamie S, Ahadiana MM, Ghiassa MA, et al. Graphene/cobalt nanocarrier for hyperthermia therapy and MRI diagnosis. *Colloids Surf B Biointerfaces*. 2016;146:271–279.
90. Liu XL, Ng CT, Chandrasekharan P, et al. Synthesis of ferromagnetic $Fe_{0.6}Mn_{0.4}O$ nanoflowers as a new class of magnetic theranostic platform for in vivo T_1-T_2 dual-mode magnetic resonance imaging and magnetic hyperthermia therapy. *Adv Healthc Mater*. 2016;5:2092–2104.
91. Herynek V, Turnovcová K, Veverka P, et al. Using ferromagnetic nanoparticles with low Curie temperature for magnetic resonance imaging-guided thermoablation. *Int J Nanomedicine*. 2016;11:3801–3811.
92. Aggarwal A, Hughes S. Palliative radiotherapy: evolving role and policy challenges. *J Cancer Policy*. 2016;10:21–29.
93. Li M, Zhao Q, Yi X, et al. Au@MnS@ZnS core/shell/shell nanoparticles for magnetic resonance imaging and enhanced cancer radiation therapy. *ACS Appl Mater Interfaces*. 2016;8:9557–9564.
94. Dou Y, Li X, Yang W, et al. Pb@Au core–satellite multifunctional nanotheranostics for magnetic resonance and computed tomography imaging in vivo and synergetic photothermal and radiosensitive therapy. *ACS Appl Mater Interfaces*. 2017;9:1263–1272.
95. Detappe A, Thomas E, Tibbitt MW, et al. Ultrasmall silica-based bismuth gadolinium nanoparticles for dual magnetic resonance–computed tomography image guided radiation therapy. *Nano Lett*. 2017;17:1733–1740.